Crustal structure of the southern part of the Baltic Sea using geophysical methods

Master Thesis

M.Sc. Program for Polar and Marine Sciences POMOR

Saint Petersburg State University / Hamburg University

by

Mikhail Vladimirov

Saint Petersburg / Hamburg, 2017

Supervisors:

Prof. Dr. Ali Dehghani, Hamburg University, Germany

Prof. Dr. Alexey Piskarev, Saint Petersburg State University, Russia

Contents

Crustal structure of the southern part of the Baltic Sea using geophysical methods

Vladimirov Mikhail

Master Program for Polar and Marine Science POMOR / 022000 Ecology and environmental management

Supervisors:

Prof. Dr. A. Dehghani, Hamburg University, Germany

Prof. Dr. A. Piskarev, Saint Petersburg State University, Russia

The study of the crustal structure of the World Ocean is very important in the many aspects. First of all, it is necessary to understand the structure of the Earth, its history, the processes of the nature which form it. When there was a need for the extraction of hydrocarbons and minerals, it was understood that studying of the crustal structure of the World Ocean is also necessary. Because, the World Ocean it is 2/3 of our planet. In the second half of the 20th century there is new problem, the global warming. Scientists realized that in order to solve this problem, is necessary knowledge in the paleoclimate, which can be obtained by studying of the sediments, crustal structure and the processes of their formation. The main source of information about the geological structure of the World Ocean floor are the results of geophysical studies. In this paper we studied the gravity data which were obtained in July 2016, in the scientific expedition AL481, on the scientific vessel RV ALKOR, the northern coast of the Rügen island, in the Baltic Sea.

The main goal of this study is to understand the crustal structure of the southern part of the Baltic Sea using geophysical methods. For a more detailed study, was decided to concentrate only on one geophysical method, gravity method. We tried to combine the previously obtained data with the gravity data obtained in the expedition AL481, interpret, and to understand whether any changes and to try, find the reason.

For the necessary result, was took gravity data, processed it, using the GRAVNAV and SEEDAT programs and obtained Free-air and Bouguer anomalies. Then, use the Oasis Montag program, Free-air and Bouguer anomalies data, were constructed of anomalies map. Further, these anomalies were interpreted using the Euler method. We calculated of the depth of bodies which creating these gravity anomalies. For comparison, we took

the gravity data, obtained in previous studies of the region, the Moho depth, the depth of the crystal basement, the depth of the intracrustal boundary, the density of sediments, the density of the upper crust, and the density of the lower crust. And also the data of geological and tectonic structure of this region and bathymetric data. Then we compare and analyze this data.

The obtained results of the gravity data from the expedition AL481 showed that, they coincide with the data obtained in previous studies of this region. But gravity data from expedition AL481 also showed new gravitational anomalies, both, negative and positive. Interpretation of these anomalies, using the Euler method, revealed the depth of the bodies which creating these gravity anomalies. Average depth of occurrence of bodies 2 - 3 km. In the west of the study area, was revealed a local values of bodies at a depth of 5 to 9 km. Comparison of the obtained results with the geological and tectonic structure of the study area allowed us the following conclusions. Considering that the study area is located in the Teicseer-Tornquist zone impact, where the West European young platform separates from the Baltic-Transdniestrian zone of pericratonic troughs in the west of the East European platform and consists of a series of deep faults, as well as in the Caledonian folding zone. The first thing that we can suppose is that in the study area there is a accumulation of fault zone and transition zone. The second is that after analyzing the southern part of the Baltic Sea, it was revealed that this is a zone of salt diapirism. The salt diapirism has the special rheological properties of the salt thickness (relatively low density, but high, especially at high pressures, plasticity). What can explain to us the negative values of gravity anomalies in the study area. In totality, transition zone , faults and salt diapirism, can lead to the formation of stratigraphic traps for hydrocarbons.

With the help of the obtained gravity results, in this study, we confirmed the heterogeneity of the gravity anomalies in the study area, the coincidence with previous studies and found a logical explanation based on geological and tectonic data of the study area. And also discovered new local gravity anomalies.

Строение земной коры южной части Балтийского моря по геофизическим данным

Владимиров Михаил

Магистерская программа «Полярные и морские исследования» («ПОМОР») / 022000

«Экология и природопользование»

Выпускная квалификационная работа магистра

Научные руководители:

Профессор, д-р Дегани А., Гамбургский университет, Германия

Профессор, д.г.н. Пискарёв А.Л., Санкт-Петербургский государственный университет, Россия

Изучение строения коры дна Мирового океана очень важно во многих аспектах. Прежде всего, это необходимо для понимания строения самой Земли, её истории, характера процессов, которые формируют её. Когда возникла потребность в добычи углеводородов и полезных ископаемых, пришло понимание того, что изучение строения коры дна Мирового океана так же необходимо. Ведь Мировой океан занимает 2 / 3 всей нашей планеты. Во второй половине XX века появилась новая проблема, глобальное потепление. Учёные поняли, что для решения данной проблемы, необходимы знания в области палеоклимата, которые можно получить при изучении донных отложений, коры дна и процессов их формирования. Основным источником информации о геологическом строении дна являются результаты геофизических исследований. В данной работе изучены гравиметрические данные, которые были получены в июле 2016 года, в научной экспедиции AL481, на научном судне ALKOR, у северного побережья острова Рюген, в Балтийском море.

Целью данной работы является изучение строение коры дна южной части Балтийского моря при помощи геофизических методов. Для более подробного исследования, было решено сконцентрироваться только на одном геофизическом методе, гравиметрическом. Мы попытались объединить полученные ранее данные с гравиметрическими данными полученными в экспедиции AL481,

интерпретировать их, и понять, произошли ли какие то изменения, и попытаться найти причину.

Для необходимого результата, были взяты гравиметрические данные, обработаны при помощи программ GRAVNAV и SEEDAT. Получены аномалии Free-air, Bouguer anomaly. Затем, при помощи программы Oasis Montag, были построены карты этих аномалий. Далее, эти аномалии были интерпретированы при помощи метода Эйлера, где была высчитана глубина залегания тел, создающих эти гравитационные аномалии. Для сравнения были взяты гравиметрические данные полученные в предыдущих исследованиях данного региона, глубина залегания границы Мохо, глубина залегания кристаллического фундамента, глубина внутрикоровой границы, плотность осадков, плотность верхней коры и плотность нижней коры. А так же данные геологического и структурно-тектонического строения данного региона и батиметрические данные. Затем проводилось сравнение и анализ.

Полученные результаты гравиметрических данных экспедиции AL481 показали, что в целом они совпадают с данными полученными в предыдущих исследованиях. Но так же показали новые гравитационные аномалии, как отрицательные, так и положительные. Интерпретация данных аномалий при помощи метода Эйлера, выявил глубину залегания тел создающих эти аномалии. Средняя глубина залегания тел 2 – 3 км. На западе района исследования, выявлено локальное нахождение тел на глубине 5 – 9 км. Сравнение полученных результатов с геологическим и структурно - тектоническим строением дна данного региона позволило сделать следующие выводы. Учитывая то, что зона исследования находится в зоне влияния Тейсейра — Торнквиста, т.е там где отделяется Западно-Европейская молодая платформа от Балтийско-Приднестровской зоны перикратонных прогибов на западе древней Восточно-Европейской платформы и состоит из серии глубинных, разломов, а так же в зоне Каледонской складчатости. Первое, что можно предположить, это то, что в зоне исследования находится скопление сдвигов и разломов. Второе, это то, что проведя анализ южной части Балтийского моря, было выявлено, что это зона соляного диапиризма. А соляной диапиризм, обусловлен особыми реологическими свойствами соляных толщ (их относительно низкой плотностью, но высокой, особенно в условиях больших давлений, пластичностью). Что нам может объяснить отрицательные значения гравитационных аномалий в зоне

исследования. В своей совокупности, сдвиги, разломы и соляной диапиризм, могут привести к образованию стратиграфических ловушек для углеводородов.

При помощи полученных результатов, в данной работе, мы подтвердили неоднородность гравитационных аномалий в зоне исследования, нашли совпадение с предыдущими исследованиями и сделали логическое объяснение, основанное на геологических и структурно-тектонических данных. А так же обнаружили новые локальные гравитационные аномалии.

1. Introduction.

1.1 Background information

Studies of crustal structure of Southern part of Northeast German Basin (NEGB), not only need to point of view, the growing needs of the hydrocarbon and mineral resources, but also from the scientific point of view. The study area is located in the southwest Baltic Sea, covering the North German Basin and the transition zone to the Baltic Shield. This is one of the most intensive researched areas in the world. Several projects were carried out to obtain a better understanding of the deep-rooted tectonic structure of the region, for example the BABEL (BABEL Working Group, 1991, 1993), DEKORP-BASIN (e.g. Meissner and Krawczyk, 1999; Krawczyk et al., 1999; DEKORP-BASIN Research Group, 1999), and POLONAISE '97 (e.g. Guterch et al., 1999; Grad et al., 1999) projects. Seismic studies in the southwestern Baltic Sea revealed evidence for Caledonian deformed younger sediments (Lassen et al., 2001; Krawczyk et al., 2002; Hansen et al., submitted for publication, Martin Bak Hansen, Magdalena Scheck-Wenderoth, Christian Hübscher, Holger Lykke-Andersen, Ali Dehghani, Benjamin Hell, Dirk Gajewski. Received 8 February 2006; received in revised form 15 January 2007; accepted 22 January 2007 Available online 12 March 2007). Structure and evolution of the northern part of the Northeast German Basin revealed from seismic interpretation and 3D structural modelling Martin Bak Hansen, 2007.

How we can see, we already have conducted quite a large amount of scientific research in the interest to us region.

In Master's thesis, we will try to combine the previously obtained and already published data with the gravity data obtained in expedition AL 481, on the research vessel ALKOR, in July 2016, to interpret them, and based on the obtained results, to understand crustal structure and modern geologic situation in this region.

The main goal of the scientific expedition AL 481 of RV 'Alkor', was to collect geophysical data, as well as recording echo-sounding bottom. The expedition was organized by the University of Hamburg, with the support of GEOMAR, Kiel and took

place in two stages, with 12.07.2016 - 20.07.2016, with one entering the seaport. The seaport of departure of the expedition was the city Kiel.

During the cruise, various geophysical data acquisition methods were used. Ship mounted instruments running nearly the full duration of the cruise included a gravimeter, measuring the gravitational field beneath the vessel, and a narrow-beam parametric sub-bottom profiler, which provided high quality data depicting the bathymetry and the stratigraphy of the uppermost sediment layers below the sea floor. Magnetometers were towed at a fixed distance behind the vessel, gathering data throughout the majority of the cruise duration. Along planned profile lines, seismic data was collected. The majority of the lines are reflection seismic profiles, the rest refraction. An airgun, running at different capacities for the two methods, and a sparker-array were used as seismic sources. From a laboratory on board, all instruments were monitored with computers and a variety of software applications, while the participants kept a watch schedule overlooking the data acquisition day and night. As well as monitoring the incoming data, it was also transferred and stored safely, and various pre-processing steps were taken.

The Northeast German Basin (NEGB) (Fig.1) is a subbasin of the Central European Basin System (CEBS) (Hansen, M., Silkeborg., 2006).

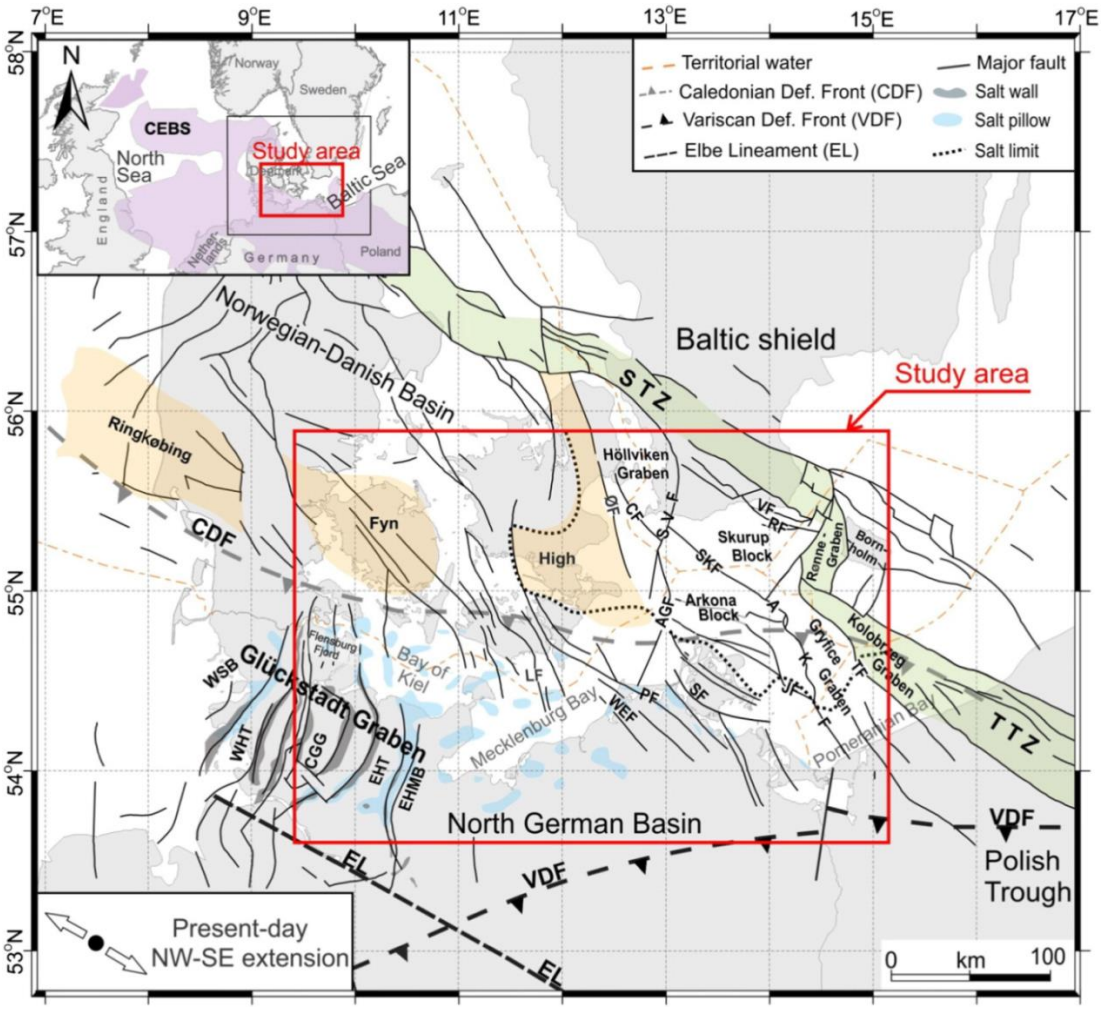

Fig.1. Location of the study area and the important structural elements of the region around the study area. Tectonic map of the Central European Basin System with the approximate location of the main structures within the study area, took from article of M. Al Hseinat and C. Hübscher., 2016, (compiled from Baldschuhn et al., 1991; Bayer et al., 1999; Clausen and Pedersen, 1999; Krauss, 1994; Kossow et al., 2000; Lokhorst et al., 1998; Maystrenko et al., 2005a; NIA, 2000; Reicherter et al., 2008; Schlüter et al., 1997; Thomas et al., 1993; Vejbæk, 1997). The present-day stress field orientation is based on Kley et al. (2008) and Kley and Voigt (2008). AGF: Agricola Fault; AKF: Adler-Kamien Fault; CF: Carlsberg Fault; CGG: Central Glückstadt Graben; EHT: Eastholstein Trough; EHMB: Eastholstein Mecklenburg Trough; JF: Jasmund Fault; LF: Langeland Fault; ØF: Øresund Fault; PF: Prerow Fault; RF: Romeleasen Fault; SF: Samtens Fault; SKF: Skurup Fault; STZ: Sorgenfrei-Tornquist Zone; SVF: Svedala Fault; TF: Trzebiatow Fault; TTZ: Teisseyre-Tornquist Zone; VF: Vomb Fault; WEF: Werre Fault; WHT:Westholstein Trough; and WSB: Westschleswig Block; M. Al Hseinat and C. Hübscher., 2016.

1.2 RV 'Alkor'.

The research vessel RV 'Alkor' belongs to Leibniz Institute of Marine Sciences IFM-GEOMAR, which is based in Kiel, Germany (Fig.2). The vessel was chartered by the University of Hamburg for the purpose of this cruise. The construction of RV

'Alkor' was completed in 1990. The vessel has an overall length of 55.20 meters, a beam width of 12.50 meters and a draught of 4.16 meters. The top cruising speed of the vessel is 12.5 knots and it has a range of up to 7,500 sm(statute miles). RV 'Alkor' can carry up to 10 crew members and at most12 scientists during a single cruise. The BRT – gross (brutto) registered tonage – of the vessel is 999.08, or the equivalent of 2,827.40 m^3.

Fig.2. The research vessel RV 'Alkor'.

1.3. Study Area.

Study area locate along the northern margin of the Central European Basin System (CEBS) in the southwestern Baltic Sea. The study area is located in at the junction of two platforms, the East European platform and the West European platform, which the Teicsea-Tornquist Line (zone) shares - the marginal seam East-European platform that separates the West European young platform from the Baltic-Transnistrian zone of pericratonic troughs in the west of the ancient East European platform.

During the Caledonian orogeny, the closure of the Tornquist Sea or the Thor Ocean, how told Berthelsen (Berthelsen, 1998) resulted in a welding together of Baltica and Avalonia. After connections of the East Avalonian terrane, the NEGB (Northeast German Basin), developed south of the Caledonian thrust belt (Meissner et al., 1994).

Several NW-SE-striking fault systems characterize the transition zone. These are, from north to south: the Tornquist Zone (TZ), the Caledonian Deformation Front (CDF) and the Trans-European Fault (TEF), which has been suggested to form the Avalonia-Baltica suture (EUGENO-S Working Group, 1988; Berthelsen, 1992) (Fig.3). Extending from the North Sea to the Black Sea, the TZ is the most major fault zone in the study area; compression, rifting and strike-slip motions (BABEL Working Group, 1991). The 20-100 km-broad TZ is lies between Rugen and Bornholm islands by pull-apart structure, the Rùnne Graben (Fig.4). The northwestern part of the Sorgenfrei-Tornquist-Zone (STZ) is an intraplate fault zone (EUGENO-S Working Group, 1988; Thybo, 1990; Franke, 1993). The southeastern part of the TZ, the Tornquist-Teisseyre-Zone (TTZ), is still interesting for study. Many scientists describe it as a plate boundary, separating Palaeozoic western Europe from the East European Platform (e.g. BABEL Working Group, 1991; Zielhuis and Nolet, 1994), but there is some evidence that it might be an intraplate fault zone (Berthelsen, 1998).

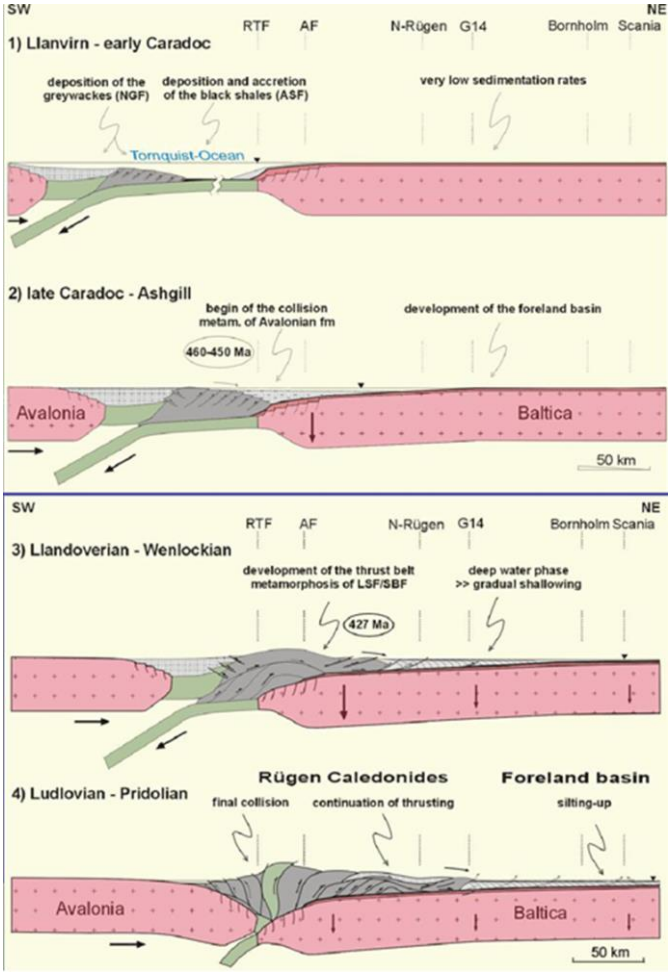

Fig.3 Caledonian deformation Baltica-Avalonia, took from article of M. Al Hseinat and C. Hübscher., 2016, (Karsten Obst, André Deutschmann1, Elisabeth Seidel and Martin Meschede, Geological Survey of Mecklenburg-Western Pomerania, University of Greifswald).

The upper crust of the NEGB consists of up to 12 km Phanerozoic sediments and thinning out northwards (DEKORP-BASIN Research Group, 1999). Between Rugen island and the Rùnne Graben, the deep borehole G14 and reflection seismic data from hydrocarbon exploration show a prominent high of the Precambrian basement overlaid by Cambrian-Silurian sediments, which unaffected by the Caledonian orogeny.

In the region of the CDF deep seismic investigations revealed NE-dipping reflectors in the upper mantle (BABEL Working Group, 1991, 1993; Meissner et al., 1994; DEKORP-BASIN Research Group, 1999), which have been interpreted as remnants of a northward subduction of the Tornquist Sea under Baltica. There are also indications of an indentation of Baltica crust (Berthelsen, 1992).

Based on these data, we see that this led to the formation of faults and blocks in the study area (Fig.1). The formation of the Vomb Fault, Romeleasen Fault, Agricola-Svedala Fault System, North Rügen Fault, Rønne Graben and the southward half grabens, such as Gryfice Graben and Kolobrzeg Graben, result from an extensive phase related to Variscan tectonics (Krauss, 1994; Krauss and Mayer, 2004; Schlüter et al., 1998).).

In the expedition AL 481, in Jule 2016, the profile measurements, was in the Baltic Sea, northern of the Rügen. West-East profiles were mainly used. In addition, North-South profiles were also used to ensure a larger coverage area and to generate cross-points. These later serve in the processing to interpolate between the profiles and to determine the drift of the sea gravimeter. The ship's GPS data were recorded and made available on an internal computer in the laboratory and used to create the overview (Fig.5), (Table.1).

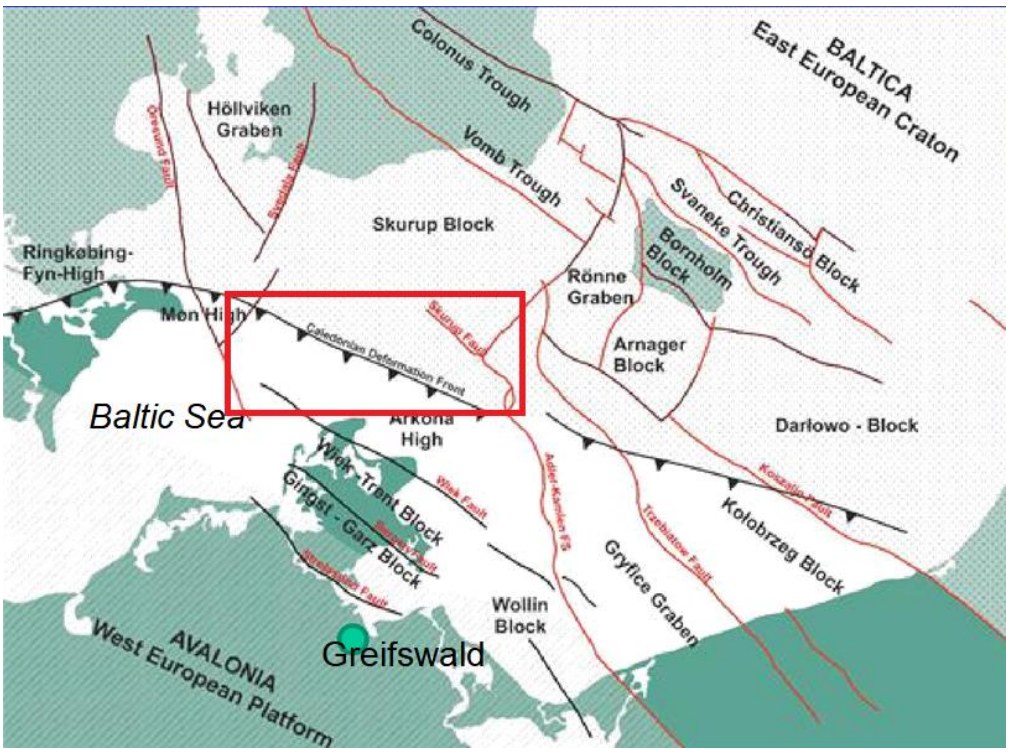

Fig.4. Karsten Obst, André Deutschmann, Elisabeth Seidel & Martin Meschede., Steps towards a 3D model of the German Baltic Sea area – collaboration with academic research in the USO project.

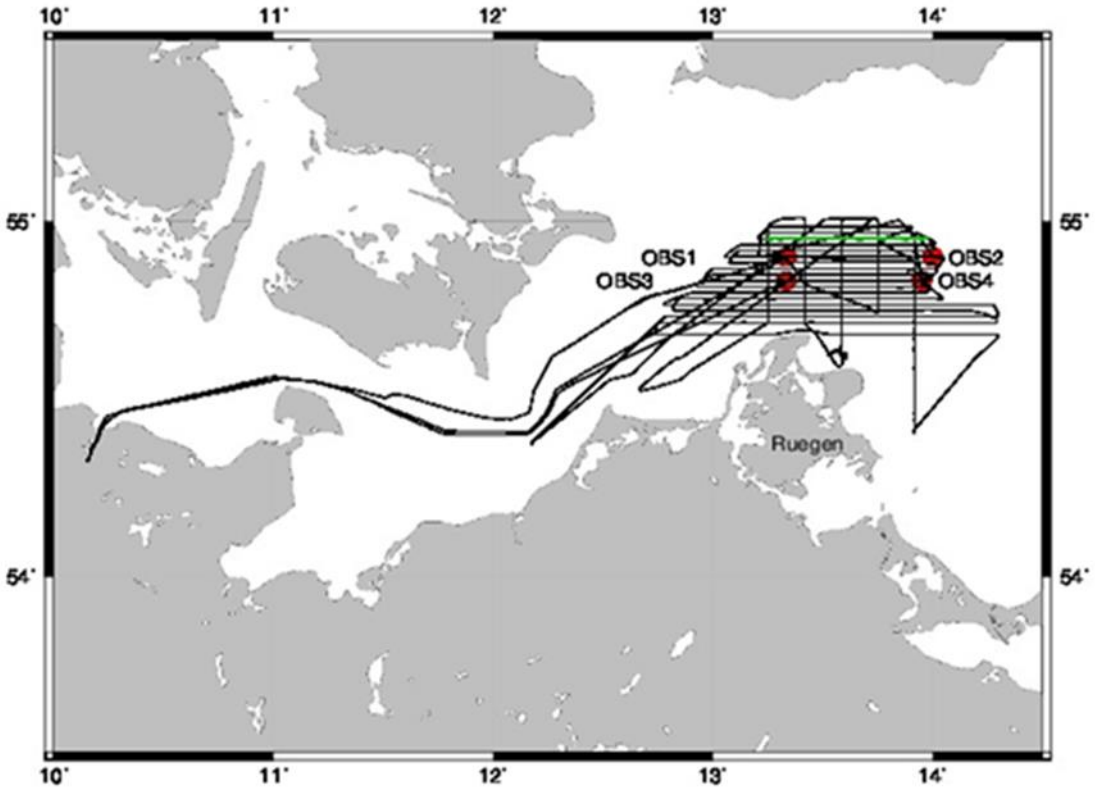

Fig.5. Maps with our cycled profiles incl. OBS positions; In green: Profile 18. The maps, was created using the Navi data and GMT.

2. Method.

2.1. Description of the Gravity method.

Gravity surveying measures variations in the Earth's gravitational field caused by differences in the density of subsurface rocks and other factors. Although known colloquially as the 'gravity' method, it is in fact the variation of the acceleration due to gravity that is measured. Gravity methods have been used most extensively in the search for oil and gas, particularly in the early twentieth century. While such methods are still employed very widely in hydrocarbon exploration, many other applications have been found (Table.2).

Hydrocarbon exploration
Monitoring of CO_2 containment underground
Regional geological studies
Exploration for, and mass determination of, mineral deposits
Detection of subsurface cavities (micro-gravity), e.g. mine Workings, caves, solution features, tunnels
Location of buried rock valleys
Determination of glacier thickness
Tidal oscillations
Archaeogeophysics (micro-gravity), e.g. location of tombs, crypts
Share of the earth (geodesy)
Satellite positioning
Monitoring volcanos
Hydrological changes in the geoid
Planetary geophysics

Table 2: Applications of gravity surveying.

Also there are micro-gravity surveys are those conducted on a very small scale of the order of hundreds of square meters - and which are capable of detecting cavities, for example, as small as 1 m in diameter within 5 m of the surface.

Perhaps the most concrete change in gravity exploration in the 1980s was the development of instrumentation that permits airborne gravity surveys to be undertaken routinely and with a high degree of accuracy. This has allowed aircraft - borne gravimeters, helicopter gravimeters to be used over otherwise inaccessible terrain and has led to the discovery of several small hydrocarbon potentials. Further advances have included the development of increasingly compact, mobile gravimeters (John M. Reynolds, 2011).

Also, recently, the rapidly evolving planetary geophysics. The Jet Propulsion Laboratory (JPL) by California Institute of Technology there is part of NASA http://www.jpl.nasa.gov/, study the solid bodies in the solar system, with particular emphasis on planets and major satellites. Research topics of JPL, include tectonics, volcanology, impact processes, geologic mapping, surface geochemistry and mineralogy, interior structure, lithosphere and mantle dynamics, gravity and magnetic field interpretation. At the center of most studies include Mars, Earth, Venus, Moon, Io, Europa, Titan, Vesta and Ceres. These bodies are studied using several methods including geophysical data interpretation.

In our study we observed marine gravity. The classical way of measuring gravity on the sea surface is by using straight line gravity meters which are installed on board of ships to measure the vertical component of the gravity field. A marine gravity meter typically consists of a gyrostabilizer platform and a gravity sensor. Different types of sensors are in use, most of which have a mass that is suspended on a metal spring to measure local differences in gravity. Thus, they measure relative differences which have to be tied to a point of known absolute gravity in a harbor (Harff., 2016).

To measure of the gravity anomalies, we used Free-air correction, *FAC* and equation Bouguer anomaly, BA.

Free-air correction, *FAC*:

$$FAC = 0{,}3086h$$

This correction $FAC = 0{,}3086h$ assumes that there is vertical gradient representing the fall-off of gravity with height for topography / bathymetry encountered on Earth.

Free-air anomaly, *FAA*

$$\text{FAA} = g_{obs} - g_{th} + 0{,}3086h \text{ mGal}$$

Where *h* is measured in meters.

Bouguer anomaly, *BA*:

$$BA = g_{obs} - g_{th} + 0.3086h - \text{Bouguer Correction}$$

Bouguer Correction, *BC*:

$$BC = 2\pi G_{ph} = 0{,}04191\ ph \text{ mGal}$$

Where h = height above sea-level datum in meters

P = density in g/cc

G = Grav. Constant = 6.672 x 10^{-11}N $m^2 kg^{-2}$

2.2. Physical background.

For our study, is necessary know the physical properties of rocks in the study area. This is necessary to understand which the density of sediment is in the study area (Fig.6), (Table.3).

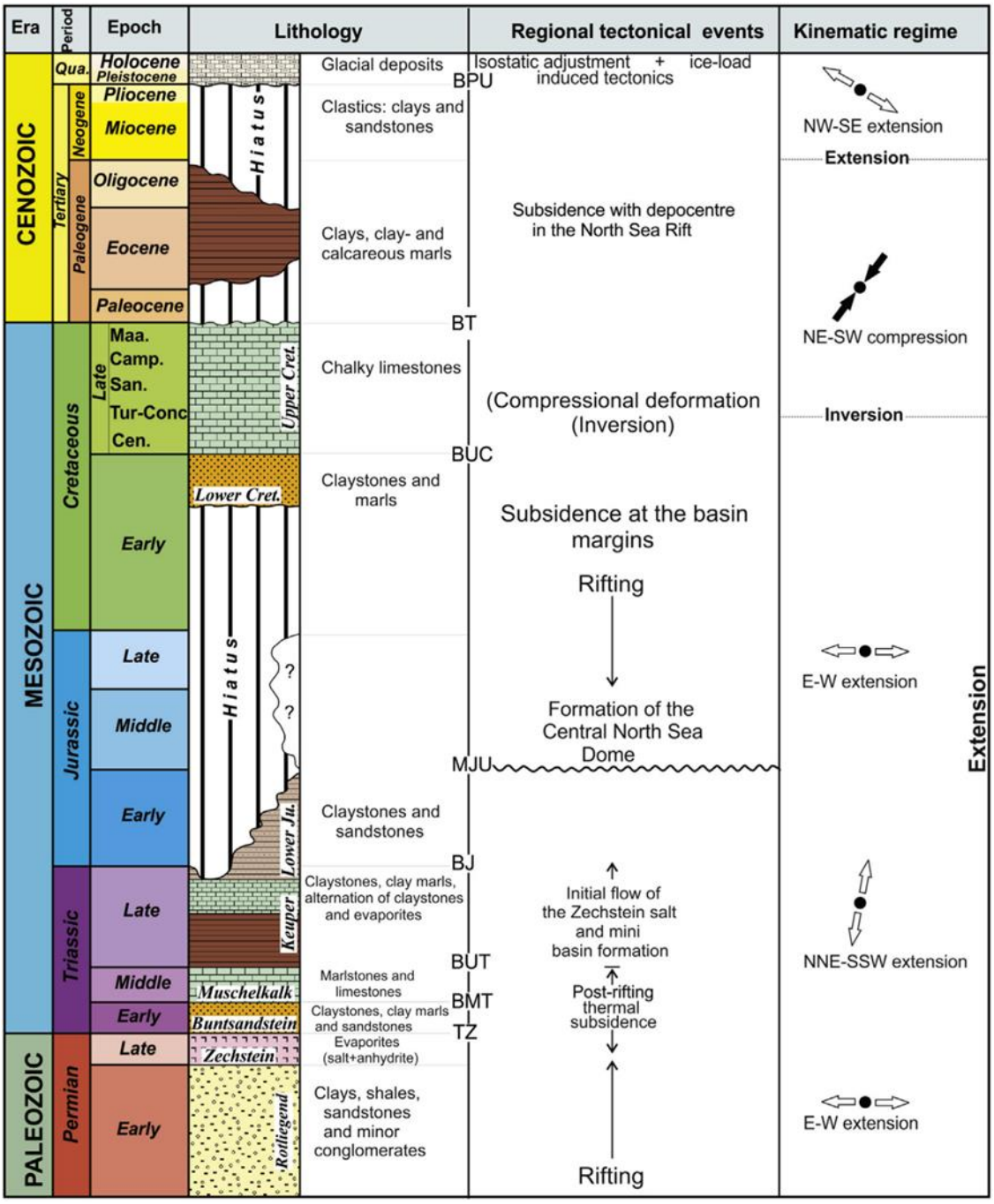

Fig. 6. Lithostratigraphic table (modified after Kossow et al., 2000) showing the dominant lithologies, main tectonic events and the ages of the major horizons interpreted along the northern margin of the North German Basin. Kinematic regime was summarized from Kley et al. (2008) and Kley and Voigt (2008). BJ: Base Jurassic; BMT: Base Middle Triassic; BPU: Base Pleistocene Unconformity; BT: Base

Tertiary; BUC: Base Upper Cretaceous; BUT: Base Upper Triassic; MJU: Mid Jurassic Unconformity; and TZ: Top Zechstein.

Stratigraphic layer	Dominant lithology	Rock density [kg/m^3]	Final porosity [%]	Initial porosity [%]	Porosity depth factor
Cenozoic	Clastics	2670	0	51	6.2
Cretaceous	Chalk	2400	0	67	6.8
Jurassic + U. Triassic	Clastics	2700	0	81	12.0
Middle Triassic	Carbonates	2400	0	20	0.5
Lower Triassic	Sandstone	2670	0	51	6.2
U. Permian Zechstein	Evaporites	2200	0	0	0
Pre-Zechstein crust	Granodiorite	2850	0	0	0
Mantle	Peridotite	3300	0	0	0

Table 3. Rock properties for the different layers used in the backstripping calculations. Hansen M., «Structure and evolution of the northern part of the Northeast German Basin revealed from seismic interpretation and 3D structural modelling», Hamburg, 2006, 95.

2.3. The equipment used to measure gravity.

During the entire duration of the cruise, gravimetric data was collected using a Bodensee gravimetric system, the Sea Gravity Sensor GSS 31 (Fig.7). This system was comprised of a gravity sensor (Fig.7 C), a control unit (Control Electronics ZEK 31M), a sensor unit (Sensor Electronics GE31M) and a power supply (Power Supply PS31M) (Fig.7 B). This system provides extremely precise measurements of the gravitational field below the vessel, and is capable of instantaneously compensating for yaw, pitch and roll of the ship.

Figure 7: A) The ship-mounted gravimetric system. B) The gravimeter control unit. C) The gravimeter.

We also used the portable gravimeter before and after the cruise. It was a La Coste & Romberg Model G No. 260 (Fig.8).

Fig.8: Ground-based measurements by gravimeter La Coste & Romberg Model G No. 260

2.4. Processing of the gravity data.

To process the data, we used special geophysical programs which was created by prof. Dr. Dehghani from Hamburg University. This are programs GRAVNAV and SEEDAT.

Firstly, we needed to combine gravity data with navigation data. We used program GRAVNAV, (Fig.9).

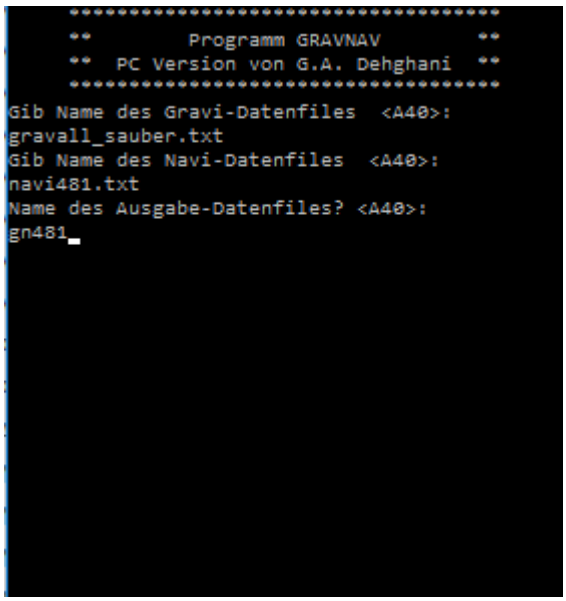

Fig.9: The screenshot of the used "GRAVNAV" program.

The received gravimetric data without processing, looked as follows (Appendix, Table.2). In (Appendix, Table.2) we can see the columns with the data. From this table we need only some data. These are: **Year, Day number, Hour, Minute, Second, Longitude, Latitude, Gravimetric data.** We called this file "**grav**".

During the expedition, was also made the bathymetric survey, and we took bathymetric and navigational data. These are: **Year, Month, Day, Hour, Minute, Second, Longitude, Latitude, Depth, Rate, Speed.** We called this file "**nav481**" (Appendix, Table.3).

Used the "GRAVNAV" program, we combined the gravity data, "**grav**" file, with the bathymetric data, "**nav**" file, and created the file "**gn481**". This is necessary in order to understand at which depths the gravitational data were obtained. See (Appendix, Table.4).

Then we counted the "Free-air" and "Bouguer" anomalies. For this we used the SEEDAT program (Fig.10).

Used the SEEDAT program, we combined the gravity-navigation data, "**gn481**" file, with the bathymetric data, "**nav**" file, and created the file "**fb481**". We got the file with the counted the "Free-air" and "Bouguer" anomalies data (Appendix, Table.5).

The next step of work, is the construction of maps, based on received data. For construction of maps, we used the Oasis montage program. First of all, we created a

relief and bathymetric map for the entire southern part of the Baltic Sea, based on the GEBCO14 digital model data (Weatherall, P., et al, 2015), (Fig.11).

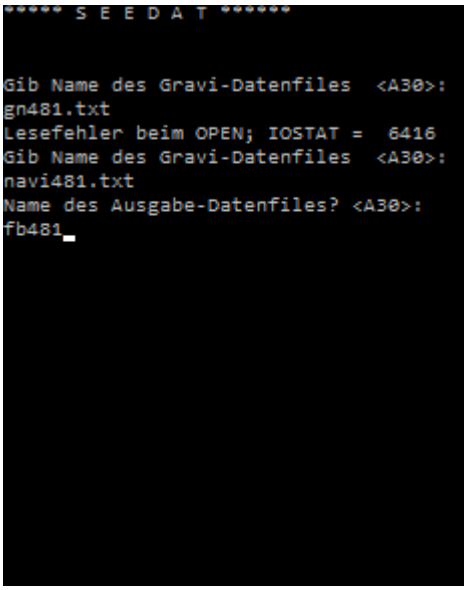

Fig.10: The screenshot of the "SEEDAT" program.

Also we needed a map of gravity anomalies throughout the southern part of the Baltic Sea in order to compare all the data and results from AL 481 expedition. We built the map on the basis of the data of the DTU15 digital models, from the Danish University, from Professor O.B. Andersen. In the model we used, the gravitational field in the Free-Air reduction (Fig.13), i.e. correction for the height of observation. For our main goal, in this field, we introduced a correction for the density of the intermediate layer between the level of the geoid, about the sea level, and the relief, the reduction of the Bouguer. The meaning of the introduction of the correction is to remove from the calculation the gravitational anomalies associated with the contrast relief of the density of the boundaries, i.e; we virtually cut the land level to sea level and filled it with sediments, with a certain density (density of the intermediate layer - 2.3 g / cm^3).

Formulas for calculation:

For land: $dGb = dGf - 0.0419*Rho*h$

For sea: $dGb = dGf - 0.0419*(Rho-Rhow)*h$

where: dGb – Bouguer anomaly (mGal), dGf – Free-air anomaly (mGal), Rho – Density of intermediate layer (2.3 g/cm^3), Rhow – Density of sea water (1.03 g/cm^3), h – mark of relief (m). (Fig.12).

Also we are created the maps of Free-air and Bouguer anomaly from data of the model DTU15 (Fig.12, Fig.13). Also we are created the maps of Free-air and Bouguer anomaly from the data and results from the AL 481 expedition (Fig.14, Fig.15), and comparative map. (Fig.16, Fig.17).

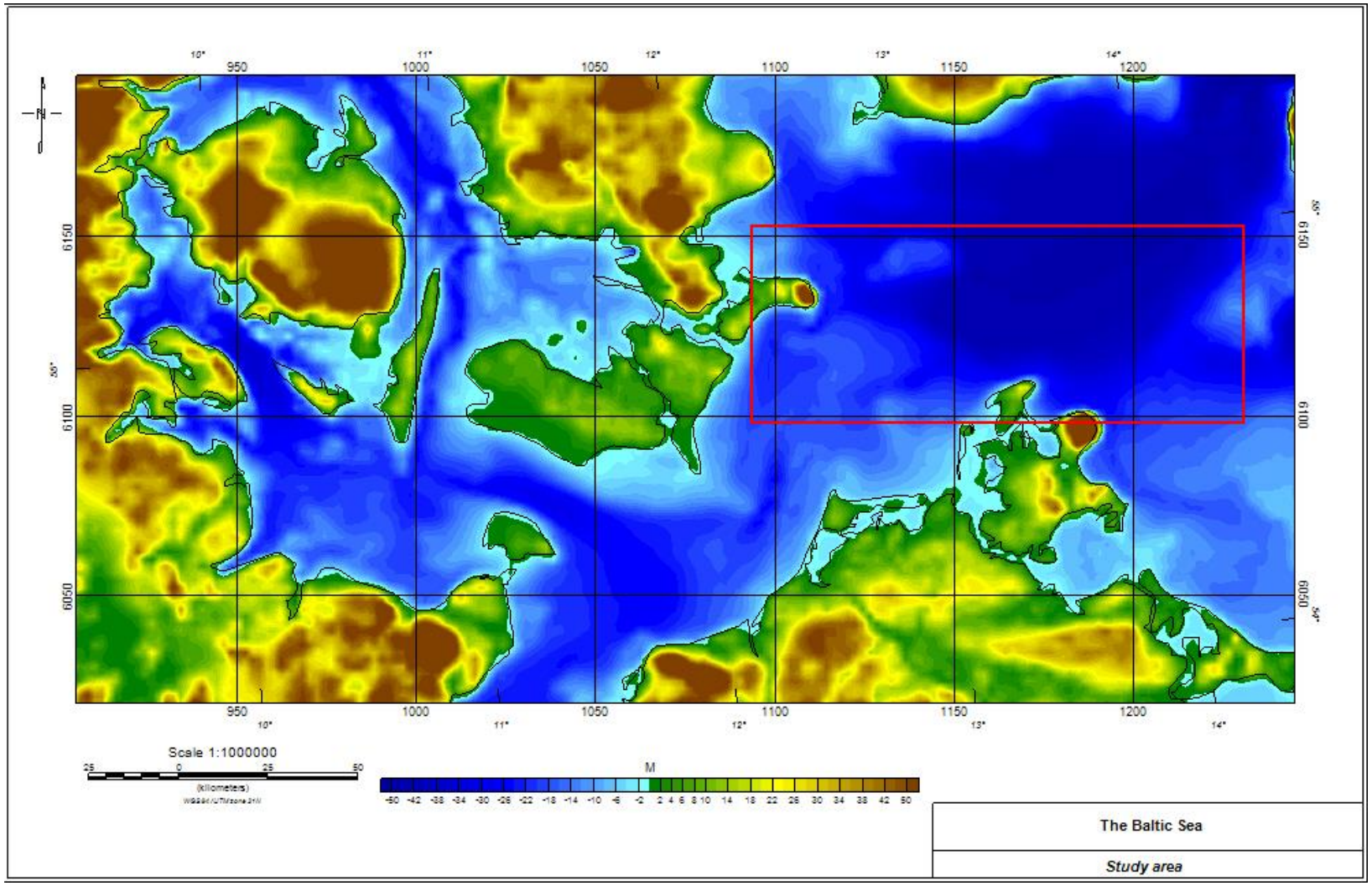

Fig.11 Bathymetric map of the study area.

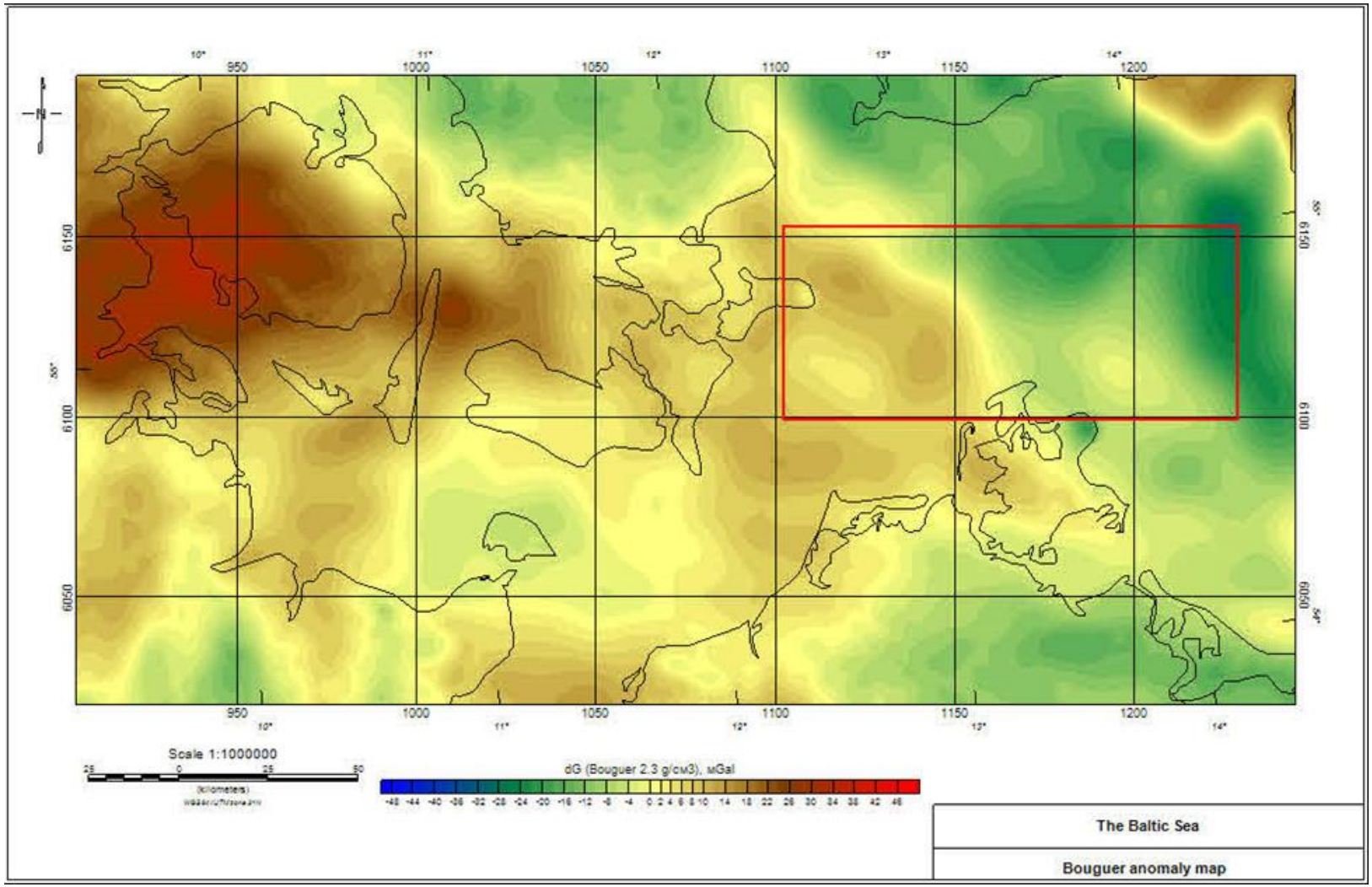

Fig.12 Bouguer anomaly map, model DTU15.

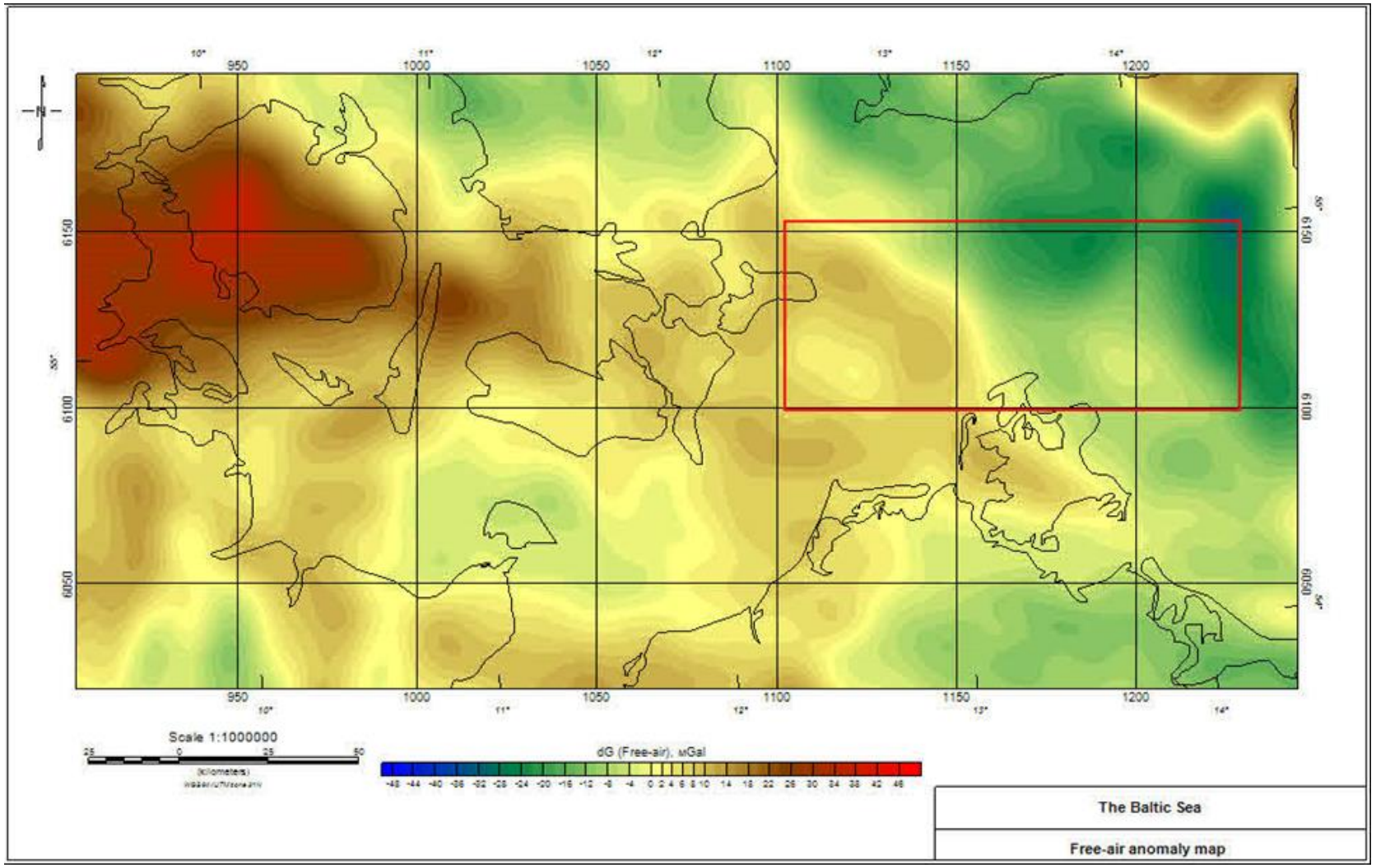

Fig.13 Free-air anomaly map, model DTU15.

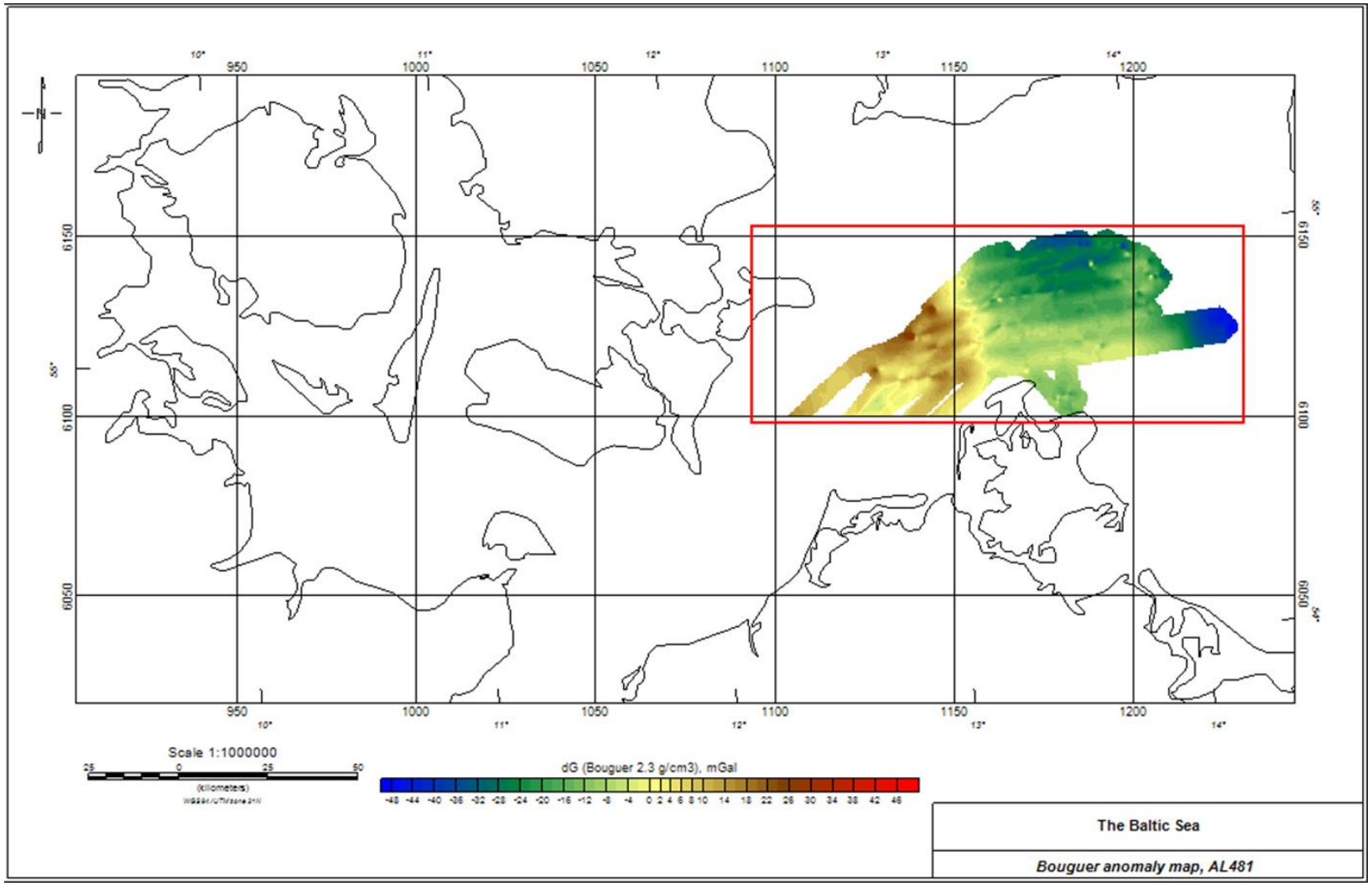

Fig.14 Bouguer anomaly map, AL481.

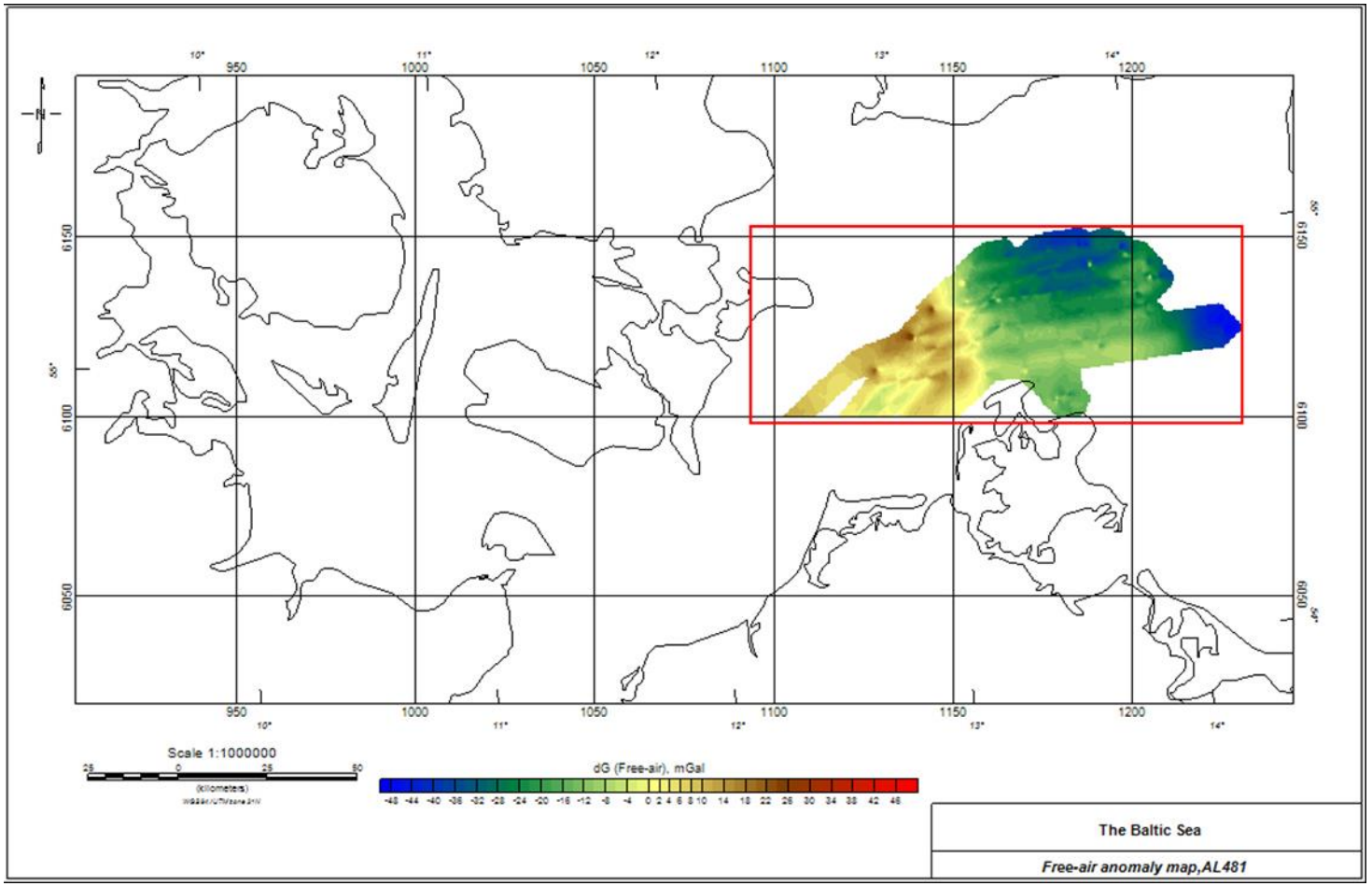

Fig.15 Free-air anomaly map, AL481.

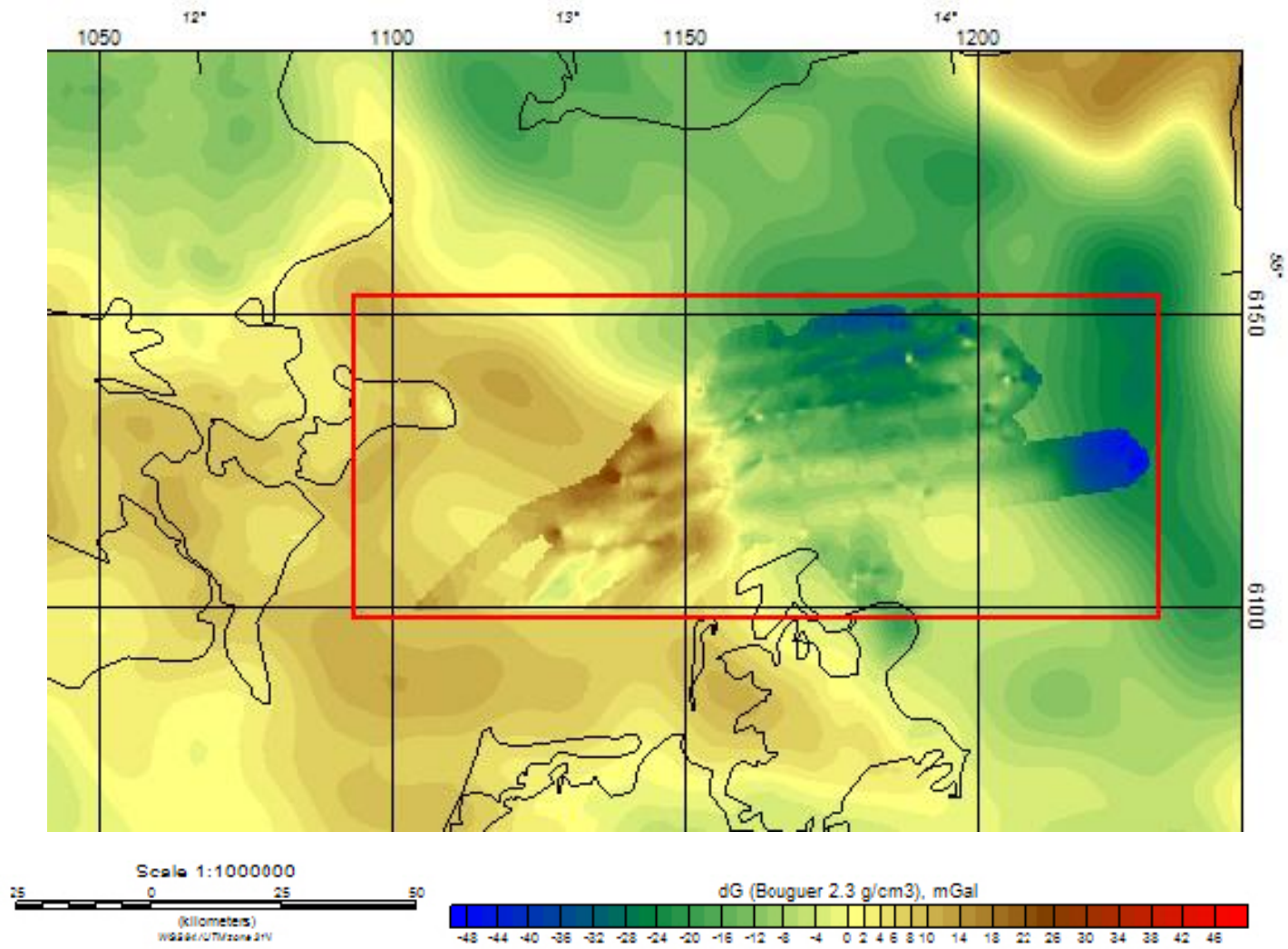

Fig.16 Bouguer anomaly comparative map.

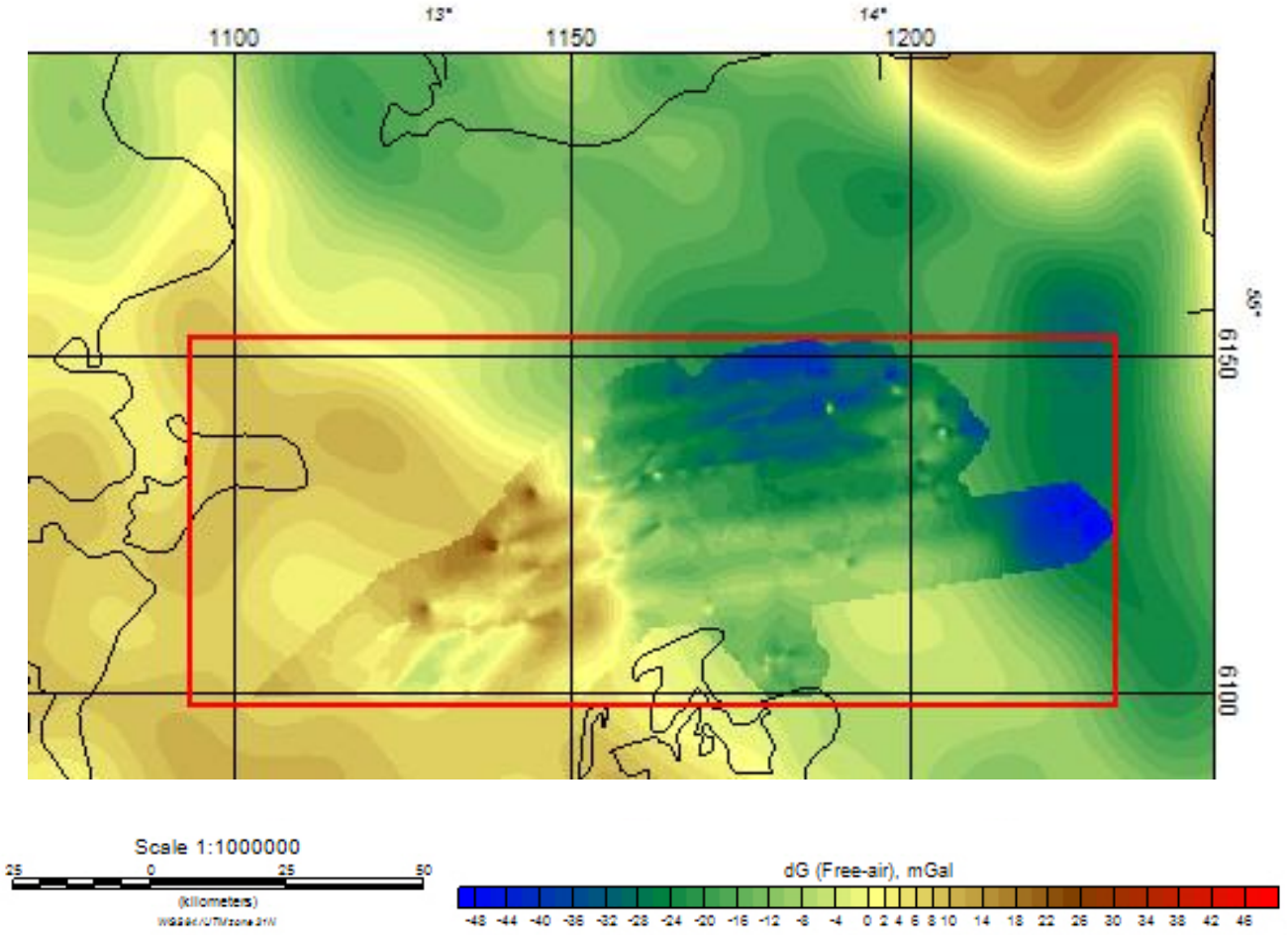

Fig.17 Free-air anomaly comparative map.

2.5. Methods of interpretation.

After the anomalies were identified, we need to interpret them. The task of interpretation, to identify the most probable distribution of density in the Earth's crust. We know that in most geological bodies have an irregular shape and an inhomogeneous density. But some geological bodies, we can describe as bodies of simple form, ball, cylinder, layer, etc. Also we can propose, that the density within this entire volume, is constant. Then, the gravitational anomalies of this bodies, can be calculated analytically. If the geological bodies have a more complex shape, different density, then only the gravity anomalies cannot be use. A more complex method is needed. It is necessary to divide complex geometric bodies into several simpler geometric bodies, and small in size with constant density. Calculate the anomalies for each such simple body separately, and compare the sum of the data of these simple anomalies with the data of the anomaly of a complex geometric body. And if these data coincide, then the assumed model of a complex body can be considered satisfactory. If they do not coincide, then gradually make changes until the difference between the anomalies become admissible.

To interpret the obtained gravity and magnetic data, we also need a complete understanding of the geological structure of the study area. For this, we needed the depths of the crustal basement, the depth of the intracrustal boundary. And of course the Moho depth boundary (Marek Grad, Timo Tiira & ESC Working Group., 2009), (Fig. 19, Fig. 20). And the density of the sediments of the region, density of the upper crust, density of the lower crust. The data, we obtained from the regional model of the crust of the Earth, EPcrust, described in the doctoral dissertation Irene Molinari, "Modeling the European crust for seismic wave propagation" (Molinari, I., Morelli, A., 2011). Based on this data, we created the necessary maps of the study area (Fig. 21, 22, 23, 24, 25). In this Master's thesis be applied Conventional 3D method. The method uses Euler's homogeneity equation to construct a system of liner equations and then solving them, in a least squares sense, for the single source of a given type. Since Euler's homogeneity equation holds not only for magnetic field itself but also for gravity fields and its derivative and a combination of derivatives, people/groups have developed Euler deconvolution of the analytical signal using the first-order or second-order vertical derivatives of the magnetic field so as to determine the structure index (SI) and/or to improve the resolution. Two advantage that Euler deconvolution has over other methods

are its easy generalization from 2D (profile analysis) to 3D (grid analysis), and its capability of directly applying to observations with variable altitudes.

The apparent depth to the magnetic or gravity source is derived from Euler's homogeneity equation (Euler deconvolution).

$$(x - x_0)\frac{\partial T}{\partial x} + (y - y_0)\frac{\partial T}{\partial y}(z - z_0)\frac{\partial T}{\partial z} = N(B - T)$$

Where T (x, y, z) is the total field magnetic in Cartesian coordinates, (x_0, y_0, z_0), the coordinates of the magnetic source, N the structural index, and B the regional field.

The first term $(x - x_0)$ ∂T/∂x of the Euler equation is the product of distance from the source $(x - x_0)$ in x coordinates and the rate of change of total field T with respect to the $x -$ direction. Normally, as $(x - x_0)$ increases, ∂T/∂x decreases. He sum of these products for all three directions is a function of $N(B - T)$ or a constant when $N = 0$.

The structural index N is basically the falloff rate of the anomaly with distance.

Model	**Mag.**	**Grav.**
Sphere (all dimensions « depth)	3	2
Line (or fault in thin beds)	2	1
Sheet edge (thickness « depth)	1	0
Block (depth extent » depth to top)	0	?

For the same structure, value of the structural index for gravity data is (N), and for magnetic data (N + 1), e.g., for a point source, gravity N = 2, and for magnetics, N = 3, which represents afield fall off of $1/r^2$ and $1/r^2$ respectively. A minus N means field increases with distance, which is not possible, so the gravity for a block is not -1. Experience suggests a value of N = 0 or 0.5 works well (Derek Fairhead., 2015)**.**

We repeat, that this method can be used both, for the interpretation of magnetic anomalies and for the interpretation of gravitational anomalies. Used this method in the program «Oasis Montag», we calculated depth of the gravity anomaly and created map Fig.17.

3. Results

We can see, that Bouguer gravity anomalies, which we got from DTU15 digital models, from the Danish University, from Professor O.B. Andersen, similar with the gravity anomaly, which we got in the expedition AL481(Fig.16). Also, we can see negative gravity anomalies in the eastern part of the study area, on the profile line from west to east, from expedition of AL481 (Fig.16). This local negative gravity anomalies, we were not observed in DTU15 digital models, from the Danish University, from Professor O.B. Andersen (Fig.12). Free-air anomaly obtained from the expedition AL481 and from DTU15, also similar (Fig.17) After interpretation, the gravity anomalies, we got the depth of bodies, which creating anomalies. Average depth of gravity anomalies 2-3 km. But also, in the eastern part of the study area, we can see the local distribution of negative anomalies with a very low coefficient of mGal, lying at the depth about 5-9 Km from expedition AL481, (Fig.18).

Also we can see that the Moho depth boundaries, has a characteristic increase, from the south-west to the northeast, in the study area (Marek Grad, Timo Tiira & ESC Working Group., 2009), (Fig.19, Fig.20).

The depth of the intracrustal boundary is reversed, in the eastern part of the study area, from the southeast to the northwest increase, and then rises again (Molinari, I., Morelli, A., 2011), (Fig.21).

The depth of the crystal basement decrease very clearly, from the south to the north (Molinari, I., Morelli, A., 2011), (Fig.22).

As for the density of sediments, density decreases, from the south-west to the northeast (Molinari, I., Morelli, A., 2011), (Fig.23).

Density of the upper crust is increase from the west to east (Molinari, I., Morelli, A., 2011), (Fig.24).

Density of the lower crust in general, it has a low density, but increases in the east of the investigated region (Molinari, I., Morelli, A., 2011), (Fig.25).

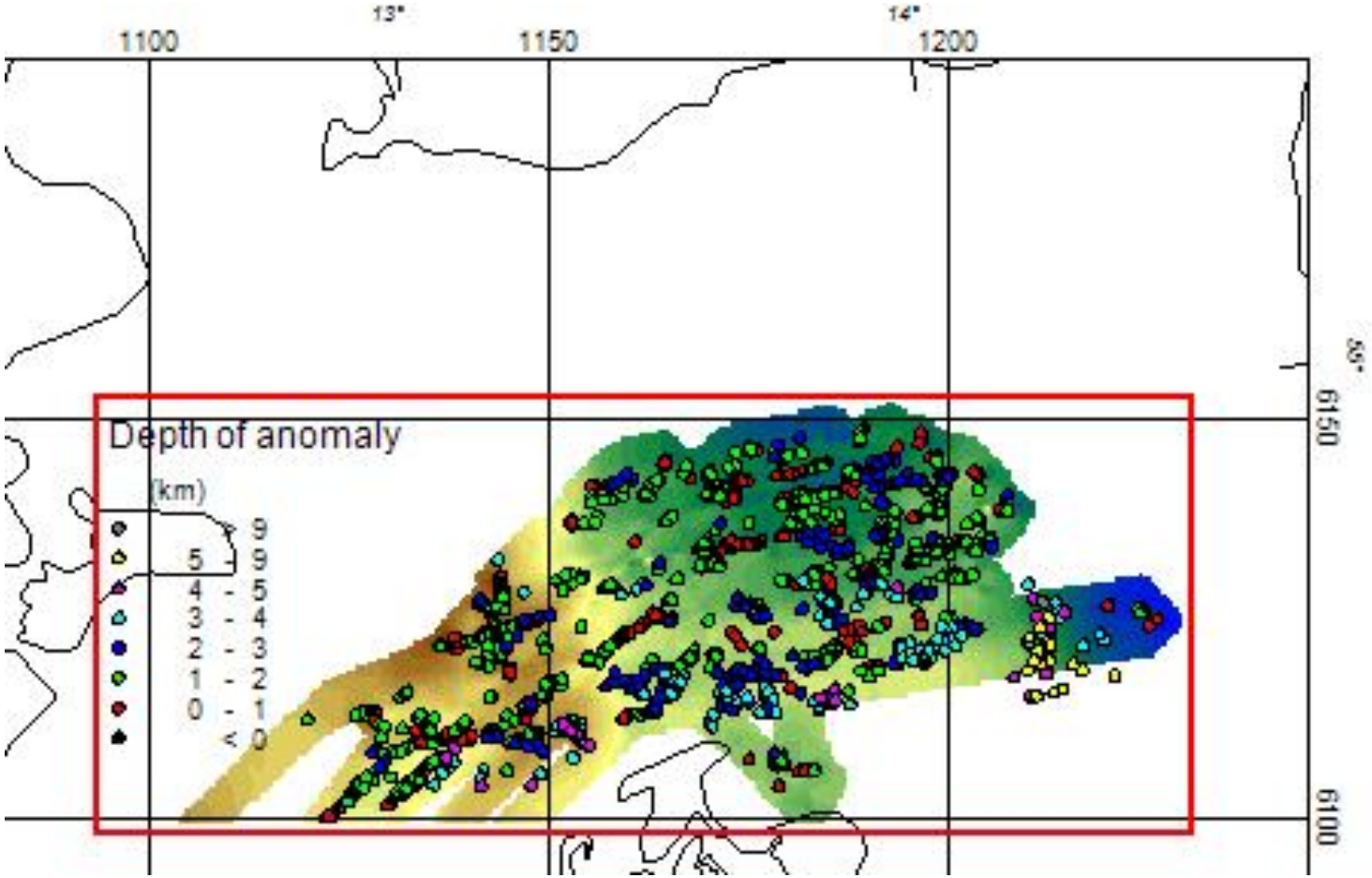

Fig.18 Map of depth of bodies sources of gravity anomaly.

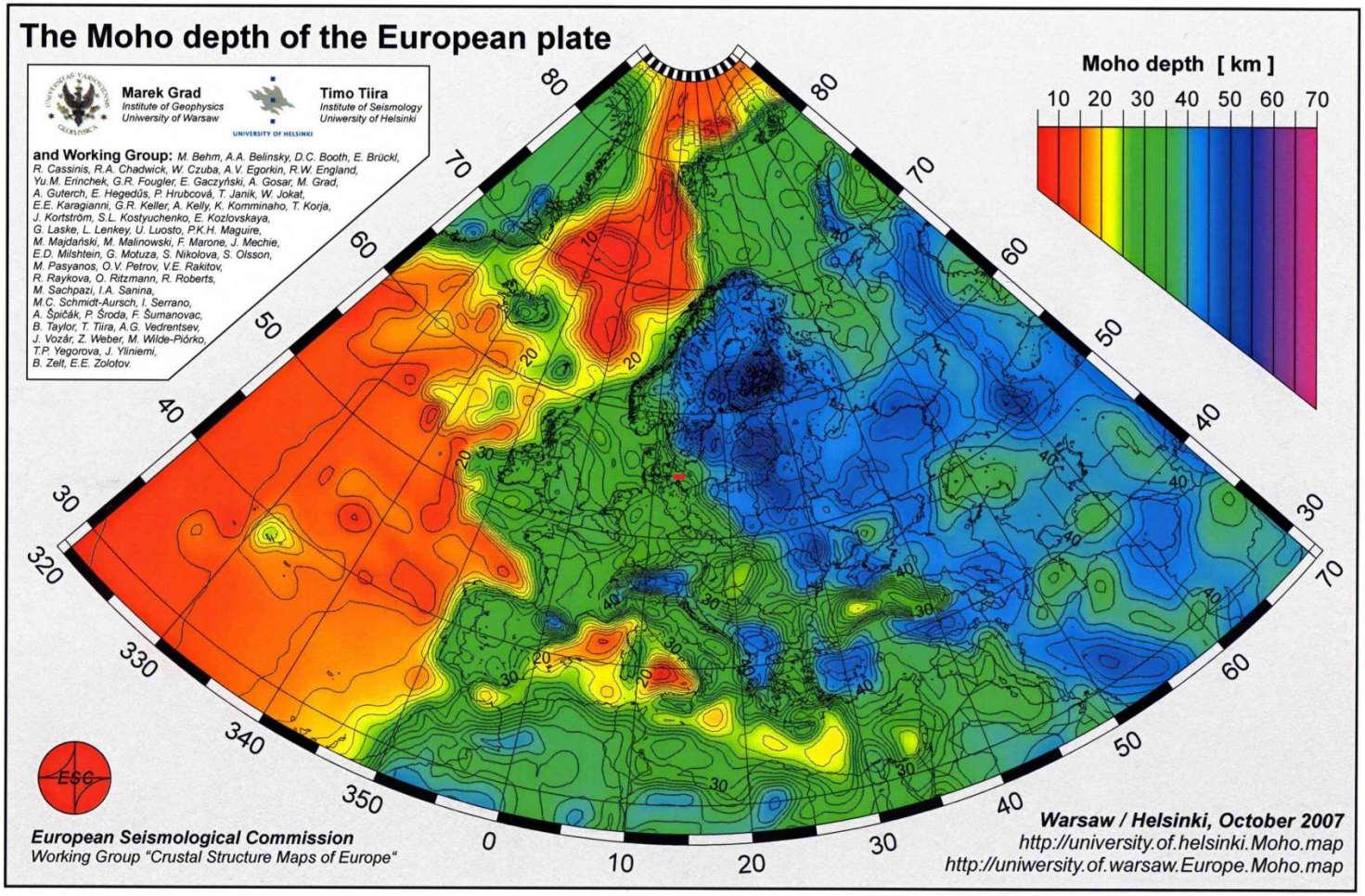

Fig.19 Moho depth of the European plate.

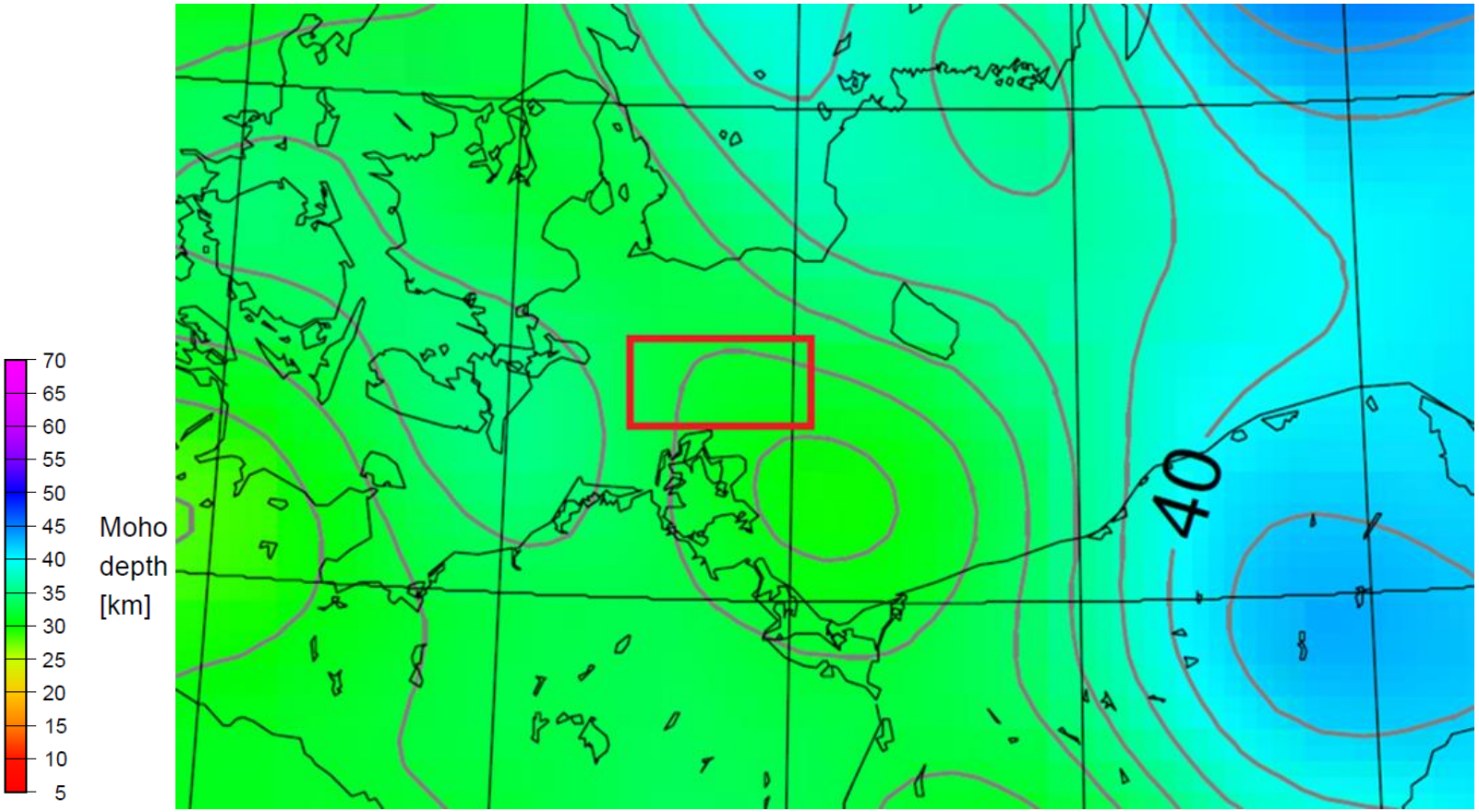

Fig.20 Moho depth of study area. (Marek Grad, Timo Tiira & ESC Working Group., 2009).

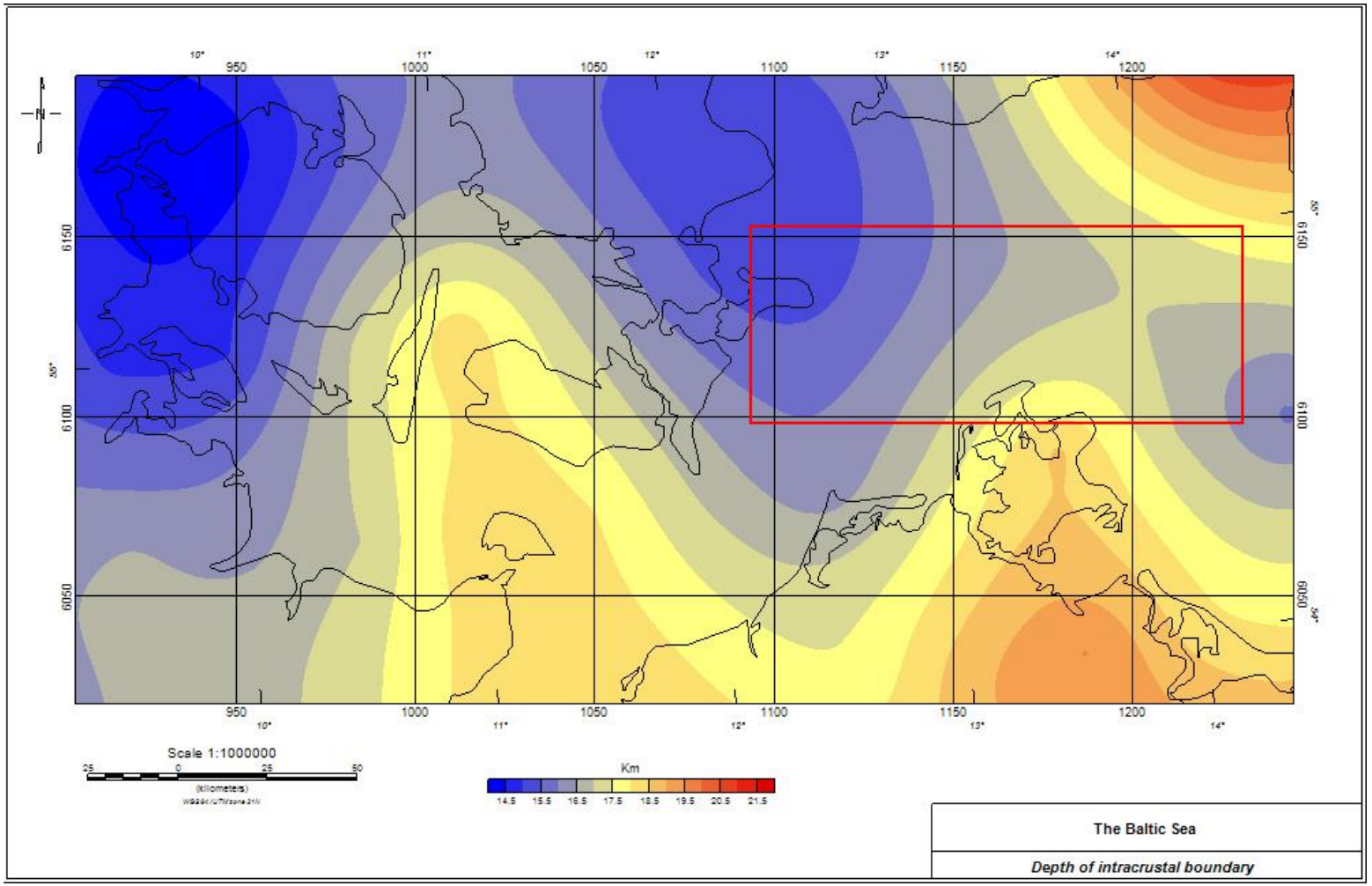

Fig.21 Depth of intracrustal boundary.

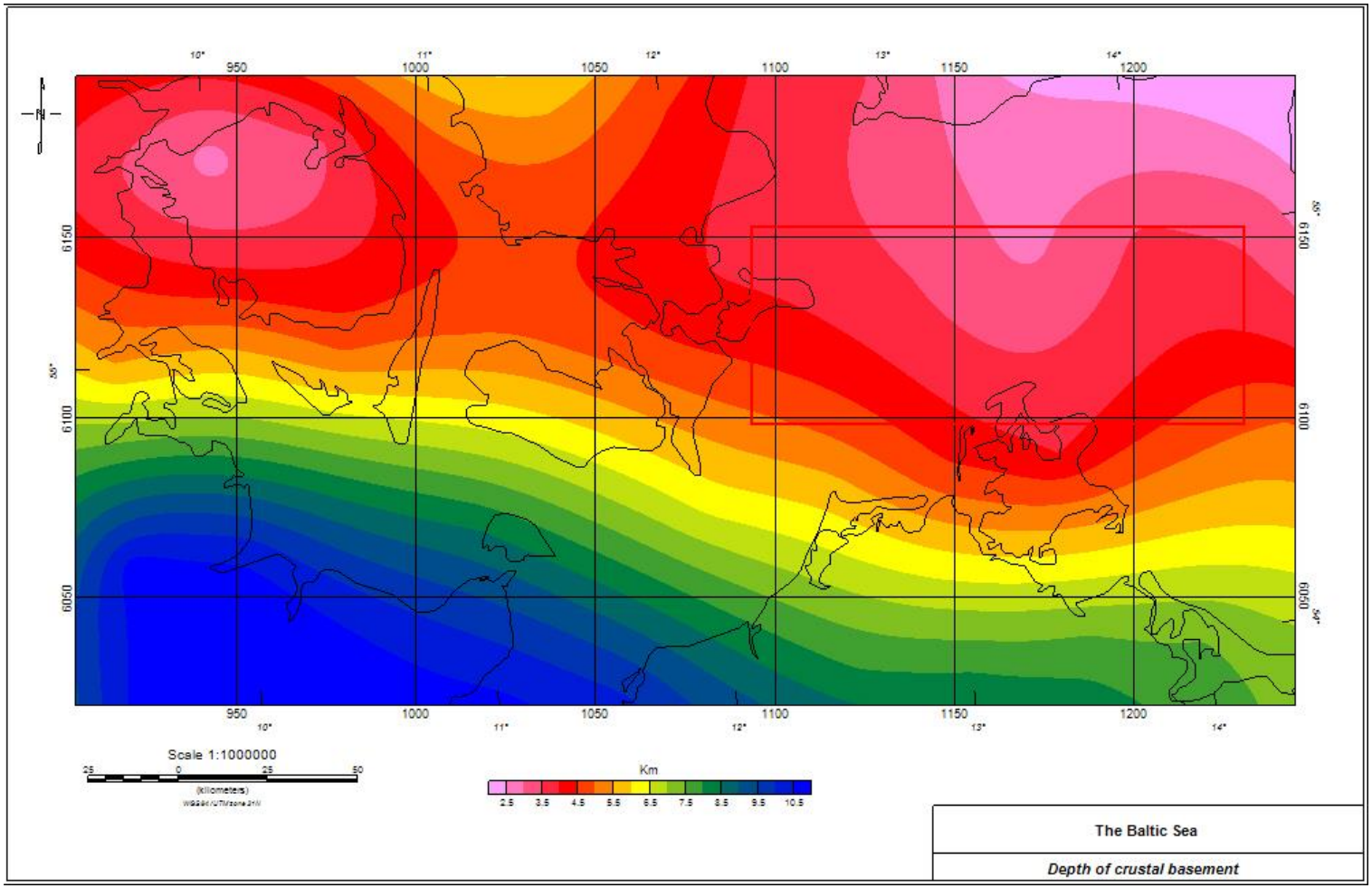

Fig.22 Depth of crustal basement.

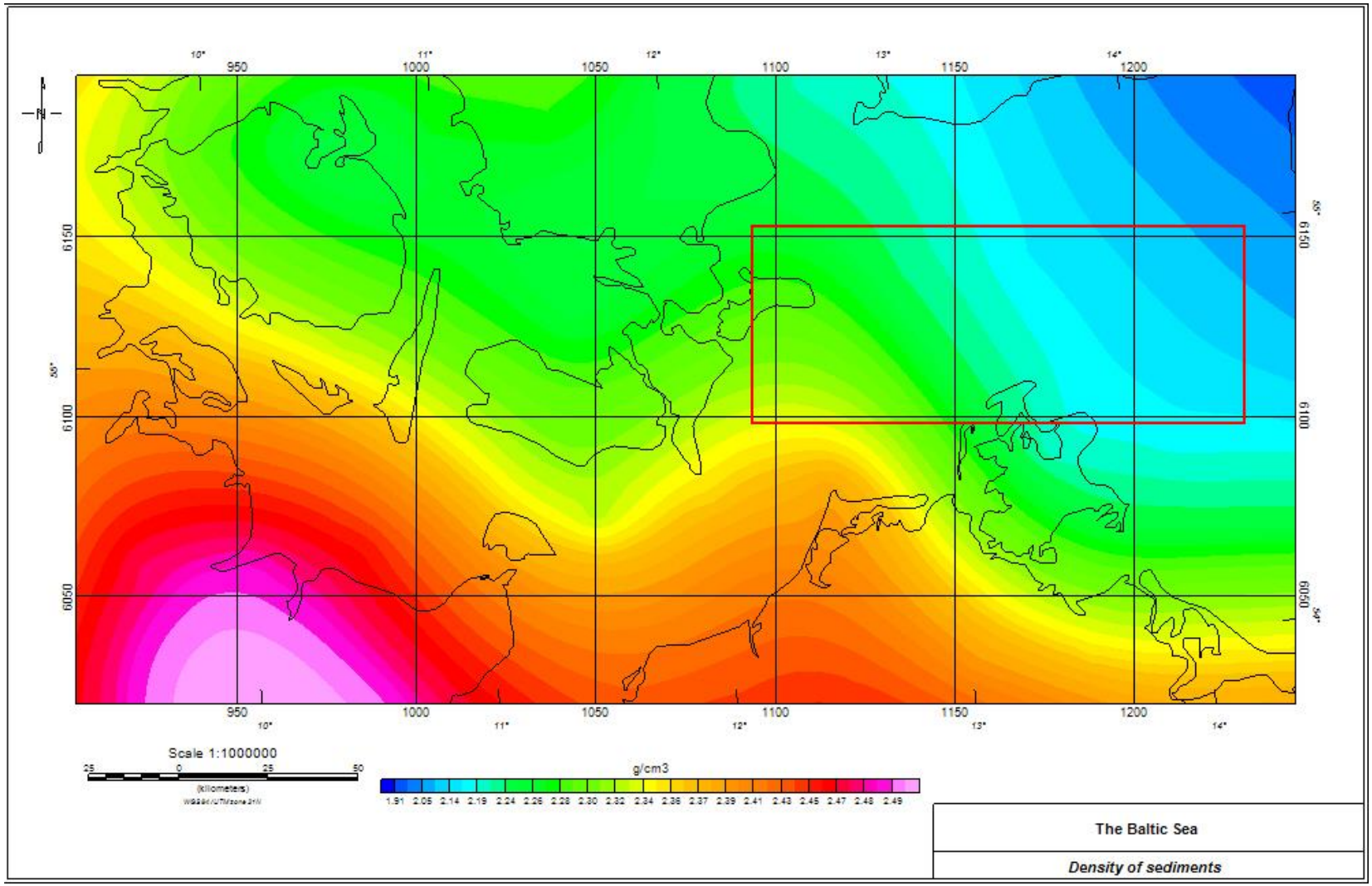

Fig.23 Density of sediments.

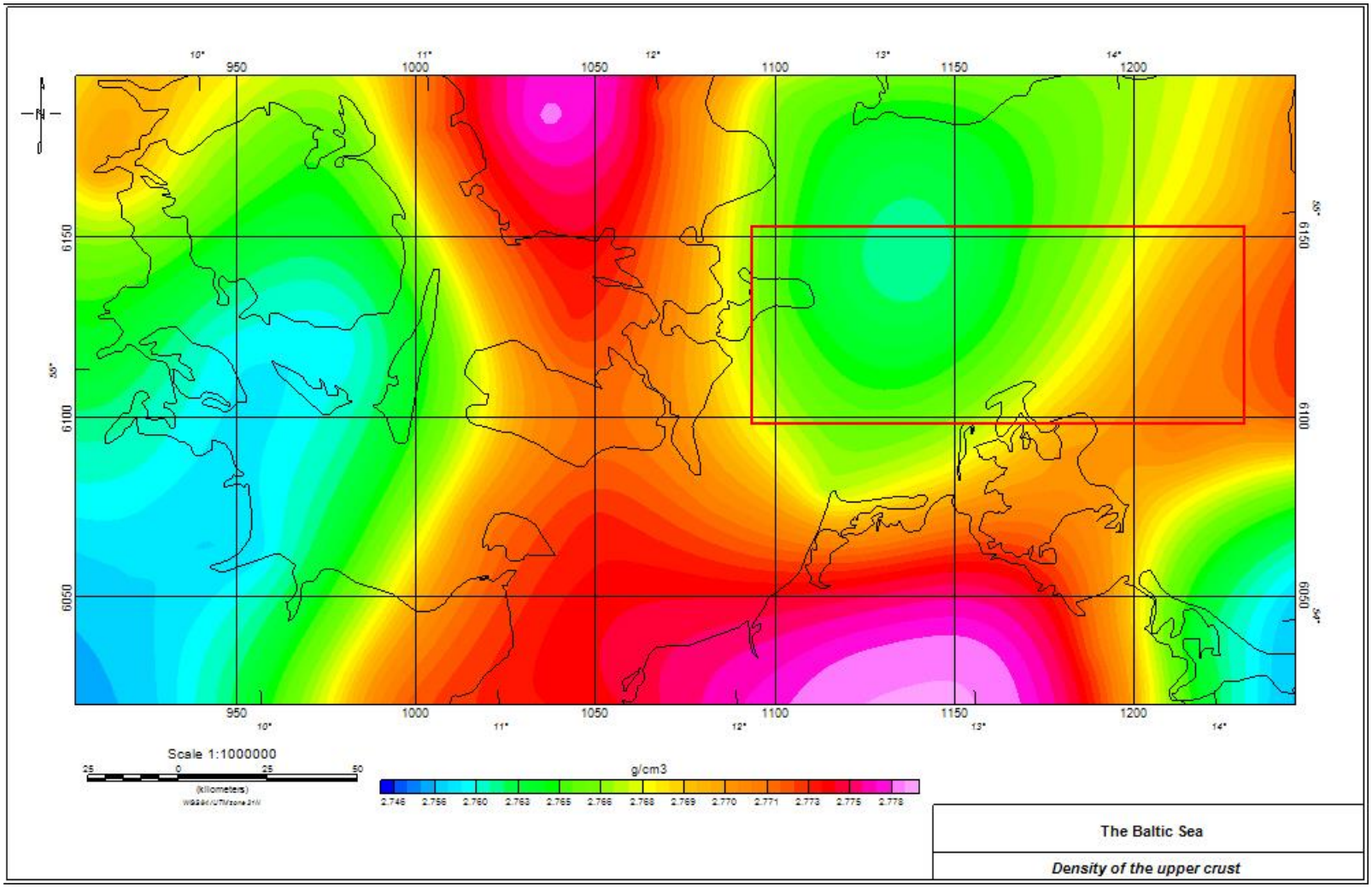

Fig.24 Density of the upper crust.

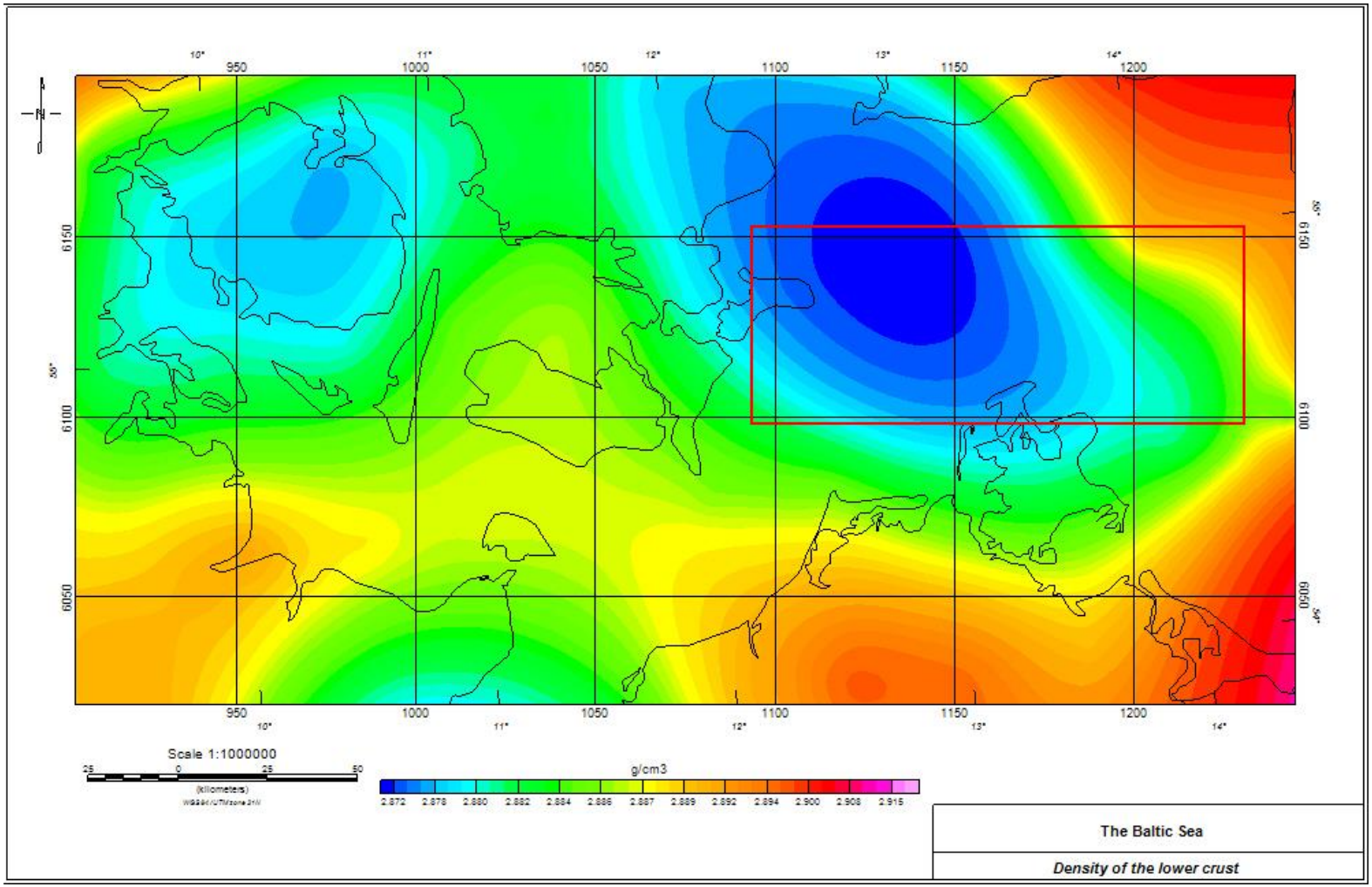

Fig.25 Density of the lower crust.

4. Discussion

The Bouguer anomaly comparative map which is based on data obtained from two sources, from the data of the DTU15 digital models, from the Danish University, from Professor O.B. Andersen, and gravity data from expedition AL481. (Fig.14 Bouguer anomaly comparative map).

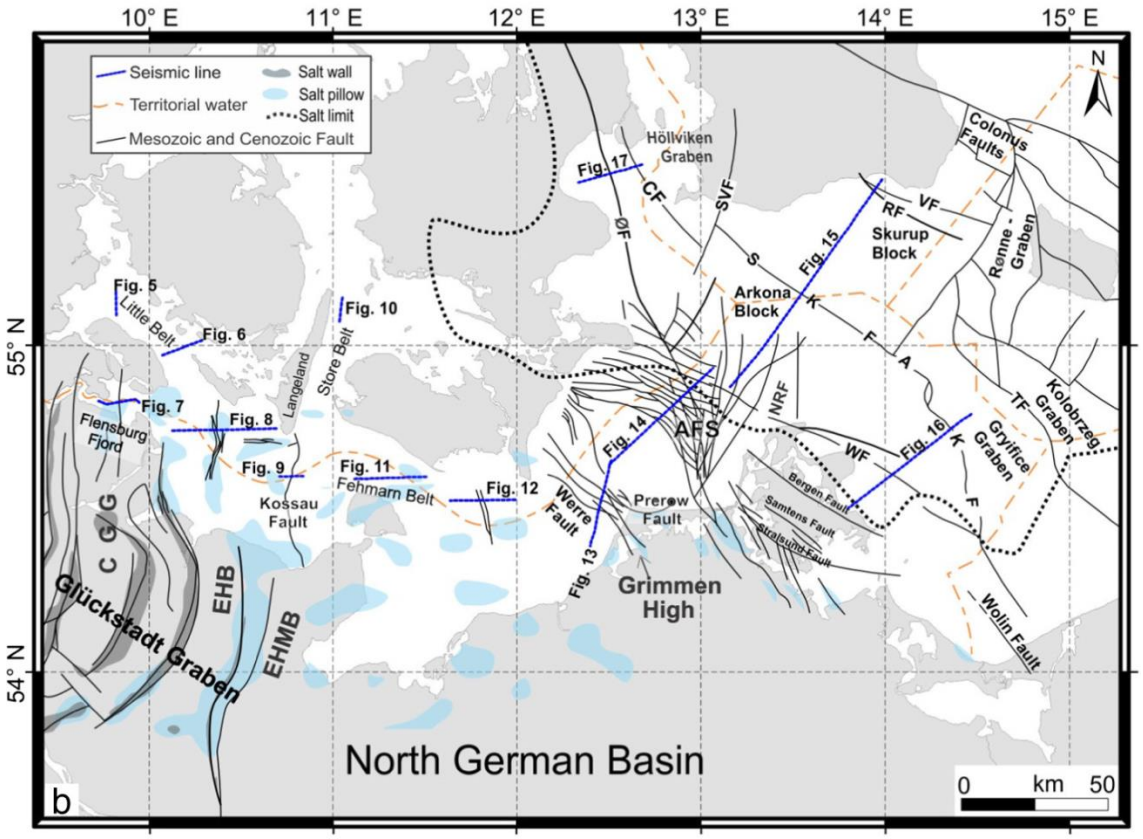

Fig.26: The distribution of salt walls and pillows (from Lokhorst et al., 1998), the locations of shownseismic profiles and Mesozoic-Cenozoic faults (compiled from AlHseinat and Hübscher, 2014; Al Hseinat et al., 2016; Hansen et al., 2005; Bayer et al., 1999; Hübscher et al., 2010; Schlüter et al., 1997, 1998). AKF: Adler-Kamien Fault; CF: Carlsberg Fault; CGG: Central Glückstadt Graben; EHT: Eastholstein Trough; EHMB: Eastholstein Mecklenburg Trough; NRD: North Rügen Fault; ØF: Øresund Fault; RF: Romeleasen Fault; SVF: Svedala Fault; VF: Vomb Fault; and TF: Trzebiatow Fault.

How we can see on this map (Fig.16), gravity anomaly fields from the data of the DTU15 is compare with the gravity anomaly fields, which we got in the expedition AL481. Also, we can see negative gravity anomalies in the eastern part of the study area, on the profile of AL481 (Fig.16). This negative gravity anomalies, were not observed in DTU15 digital models, from the Danish University, from Professor O.B. Andersen (Fig.12). After interpretation of the gravity anomalies, we got the depth of bodies, creating anomalies. Average depth of gravity anomalies sources 0-3 km. But

also, in the eastern part of the study area, we can see the local distribution of sources high negative anomalies in mGal, lying at the depth about 4-9 Km from expedition AL481, (Fig.18). Changes of the gravity anomalies can be caused by many factors. Haw we can see, the Moho depth boundaries, has a characteristic increase, from the south-west to the northeast, in the study area. What can to lead to increase of the thickness of the crust(Marek Grad, Timo Tiira & ESC Working Group., 2009), (Fig. 19, Fig.20). The raise of the crustal basement, and deformation of depth of intracrustal boundary, which we can see on (Fig.21, Fig.22), (Molinari, I., Morelli, A., 2011). can be a consequence of the tectonic movement, which we can see in column «Kinematic regime» on (Fig.6) in Lithostratigraphic table (modified after Kossow et al., 2000) showing the main tectonic events and the ages of the along the northern margin of the North German Basin, which can leded to the rise of the crustal basement, and deformation of depth of intracrustal boundary, which we can see on (Fig.21, Fig.22), (Molinari, I., Morelli, A., 2011). . The depth of the intracrustal border is reversed, in the eastern part of the study area, from the southeast to the northwest increase, and then rises again (Figure 21), (Molinari, I., Morelli, A., 2011). The depth of the crystal basement decrease very clearly, from the south to the north. (Fig.22), (Molinari, I., Morelli, A., 2011). As we can see, the density of the lower crust in the study area, is higher than the density of the upper crust. Both crusts has trend to increase to the east. But in generally, they are compensate each other (Fig.24, Fig.25) (Molinari, I., Morelli, A., 2011). Including all these factors, we think that TTZ: Teisseyre-Tornquist Zone, major faults and CDF: Caledonian deformation front influence on study area.

As for the density of sediments, density decreases, from the south-west to the northeast. If we are compare the map of the density of sediments and the map of gravity anomalies, we can see that with decreasing density of sediments (Fig.23), (Molinari, I., Morelli, A., 2011), gravity anomalies decrease, from the south-west to the northeast (Fig.16).

Nevertheless, in the east of the study area, we have characteristically low gravity anomalies on the depth 0 – 3 Km, including very low, local gravity anomalies on the depth 4 – 9 Km. (Fig.18). Logically the presence of a salt extrusion induces a negative gravity anomaly due to its physical properties, mainly its density. As we know, salt structures in Northern Germany very extensive in Germany (Fig.26, Fig.27), (Lokhorst et al., 1998), (Bundesanstalt f. Geowissenschaften u. Rohstoffe., 2008).

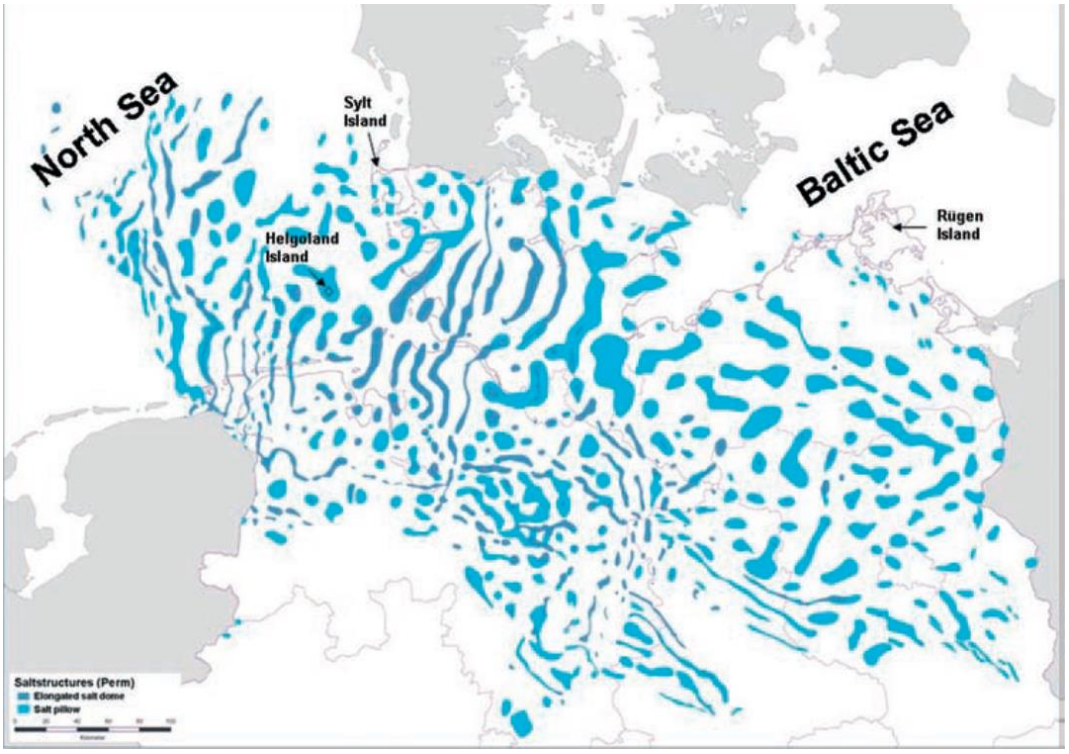

Fig.27: Salt structures in Northern Germany (Bundesanstalt f. Geowissenschaften u. Rohstoffe (2008), modified.

Salt diapir is a multiform-shaped body of crystalline aggregate of evaporite minerals (mainly halite) that has contacts with the encompassing sedimentary strata and formed due to salt movement. The process of salt diapir formation, often referred to as diapirism, is accompanied by deformations significant in scale and magnitude of both, rocks and salt itself. It is the phenomenon which we known as salt tectonics, or halokinesis. There are several ways to characterize the salt diapirs. The most common classifications are based on morphological characteristics of the features and on inferred mechanisms of their formation. (Jackson and Talbot., 1991) characterized the salt diapirs as masses of salt that have flowed ductilely and appear to intruded the overburden. Diapirs begin as anticlinal or domal uplifts and evolve into pillows, domes, and mushroom-shaped diapirs, columns, canopies, bulbs, tongues, walls, and more complex features (Fig.28), (Hudec and Jackson., 2007).

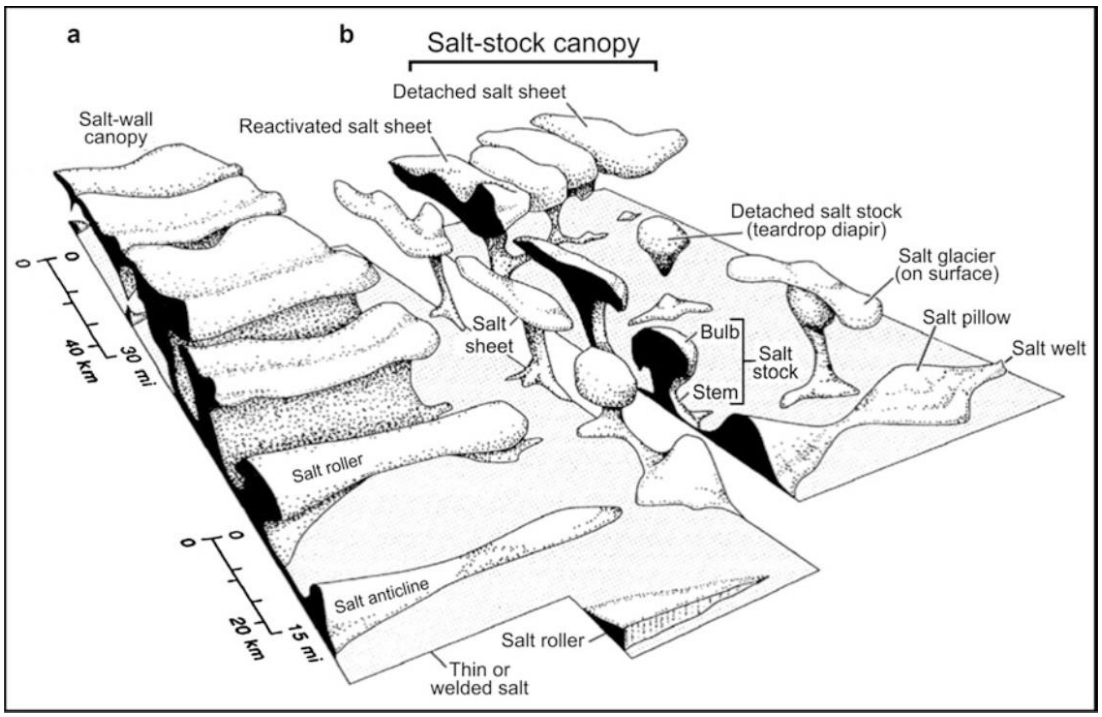

Fig.28. Salt Diapirism in the Oceans and Continental Margins, Figure 2 Main types of salt structures that develop from linear sources (a) and point sources (b) (modified from Hudec and Jackson 2007).

Dynamically, the salt diapirs, can develop of different ways, reactive, active, passive, or dormant (Yin and Groshong., 2006). (Fig.29) illustrates different stages of the diapir formation. The diapirism can develop triggered when the overburden rocks are subjected to extension, compression, uplift, and erosion (reactive diapirism). Very often salt rises in the basewalls of normal faults where the sedimentation rate remains low (Vendeville and Jackson., 1992; Quirk and Pilcher., 2012). The faulted overburden lets a reactive diaper move up (Fig.29), (Hudec and Jackson 2007). This gives way to an active diapirism (b). When salt attains the surface, it can continue to rise by passive diapirism (c), in which the diaper grows as sediments accumulate around it. A rapidly rising passive diapir may spread over the sediment surface to form an allochthonous salt sheet (d). According to Koyi (1998), the salt diapir geometry may be the result of different combinations, namely, the rates of sediment accumulation, rate of salt supply, and rates of extension/erosion/dissolution/shortening at different times (Drachev, Sergey S. 2014).

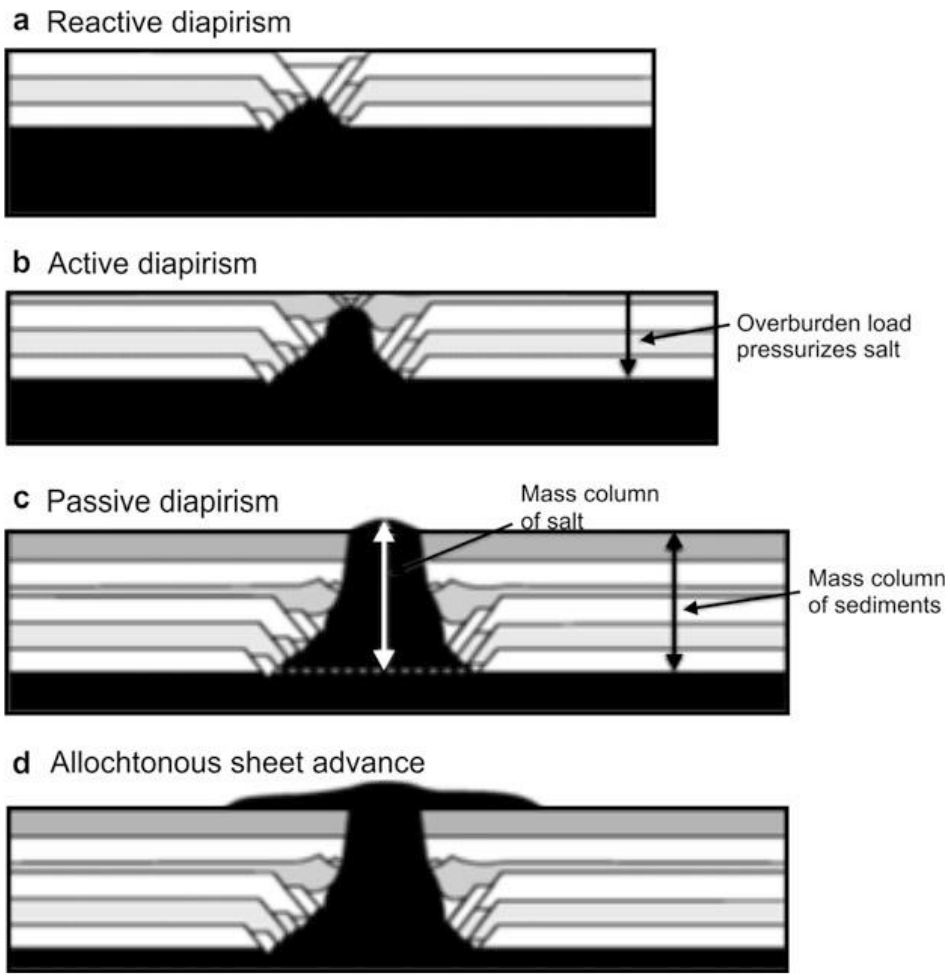

Fig.29: Salt Diapirism in the Oceans and Continental Margins. Progressive development of a diapir from reactive to passive stage. Black represents the salt layer and white-gray layers sedimentary overburden (modified from Hudec and Jackson 2007).

The initiation of salt diapirs can be realized by several driving forces and/or their combinations including buoyancy, tectonic stresses, gravity-driven gliding or differential loading (Hudec and Jackson, 2007).

In our case, initiation of salt diapirs can be TTZ: Teisseyre-Tornquist Zone, major faults and CDF: Caledonian deformation front.

5. Conclusions.

We think that gravity anomalies are caused by salt diaperide. But initiation of salt diapirs can be TTZ: Teisseyre-Tornquist Zone, major faults and CDF: Caledonian deformation front. The Moho depth increase from 34 Km to 36 Km. Also we can see the raise of the crustal basement, and deformation of depth of intracrustal boundary. The depth of the intracrustal border is reversed, in the eastern part of the study area, from the southeast to the northwest increase, and then rises again. The depth of the crystal basement decrease very clearly, from the south to the north. As we can see, the density of the lower crust in the study area, is higher than the density of the upper crust. Both crusts has trend to increase to the east. As for the density of sediments, density decreases, from the south-west to the northeast. If we are compare the map of the density of sediments and the map of gravity anomalies, we can see that with decreasing density of sediments, gravity anomalies decrease, from the south-west to the northeast.

But first of all, only complex of geophysic study, like gravity survey, magnetic survey, seismic survey, will help for us understand the history of the development of this region.

6. References

Al Hseinat, M., et al. "Triassic to recent tectonic evolution of a crestal collapse graben above a salt-cored anticline in the Glückstadt Graben/North German Basin." Tectonophysics 680 (2016): 50-66.

BABEL Working Group. "Deep seismic reflection/refraction interpretation of crustal structure along BABEL profiles A and B in the southern Baltic Sea." Geophysical Journal International 112.3 (1993): 325-343.

Baldschuhn, R., Best, G., Kockel, F., 1991. Inversion tectonics in the North-west German Basin. In: Spencer, A.M. (Ed.), Generation, Accumulation and Production of Europe's Hydrocarbons. Special Publication of the European Association of Petroleum Geoscientists. Vol. 1, pp. 149–159.

Bayer, U., Scheck, M., Rabbel, W., Krawczyk, C.M., Götze, H.J., Stiller, M., Beilecke, T., Marotta, A.M., Barrio-Alvers, L., Kuder, J., 1999. An integrated study of the NE-German Basin. Tectonophysics 314, 285–307.

Berthelsen, " Avalonia-Baltica suture", 1992, EUGENO-S Working Group, 1988.

Berthelsen, Asger. "The Tornquist Zone northwest of the Carpathians: an intraplate pseudosuture." Gff 120.2 (1998): 223-230.

Berthelsen, Asger. "The Tornquist Zone northwest of the Carpathians: an intraplate pseudosuture." Gff 120.2 (1998): 223-230.

Clausen, O.R., Pedersen, P.K., 1999. The Triassic structural evolution of the southern margin of the Ringkøbing-Fyn High, Denmark. Mar. Pet. Geol. 16, 653–665.

DEKORP-Basin Research Group. "Deep crustal structure of the Northeast German basin: New DEKORP-BASIN'96 deep-profiling results." Geology 27 (1999): 55.

Derek, j., Fairhead. 2015. Advances in Gravity and Magnetic Processing and Interpretation, 250 - 265, EAGE Publications bv.

Drachev, Sergey S. "Salt Diapirism in the Oceans and Continental Margins." Encyclopedia of Marine Geosciences (2014): 1-8.

Eugeno-S Working Group. "Crustal structure and tectonic evolution european of the transition between the Baltic Shield and the North German Caledonides (the EUGENO-S Project)." Tectonophysics 150.3 (1988): 253-348.

Franke, Dietrich. "The southern border of Baltica—a review of the present state of knowledge." Precambrian Research 64.1-4 (1993): 419-430.

Geol. Wiss. 22, 19–32.

Hansen M., «Structure and evolution of the northern part of the Northeast German Basin revealed from seismic interpretation and 3D structural modelling», Hamburg, 2006, 95.

Hansen, M., aus Silkeborg, Structure and evolution of the northern part of the Northeast German Basin revealed from seismic interpretation and 3D structural modelling. Dissertation zur Erlangung des Doktorgrades der Naturwissenschaften im Fachbereich Geowissenschaften, der Universität Hamburg Dänemark; Hamburg, 2006.

Hansen, M., Magdalena Scheck-Wenderoth b, Christian Hübscher a, Holger Lykke-Andersen c, Ali Dehghani a, Benjamin Hell a, Dirk Gajewski. Basin evolution of the northern part of the Northeast German Basin — Insights from a 3D structural model. Received 8 February 2006; received in revised form 15 January 2007; accepted 22 January 2007 Available online 12 March 2007.

Hansen, Martin Bak, et al. "Basin evolution of the northern part of the Northeast German Basin—Insights from a 3D structural model." Tectonophysics 437.1 (2007): 1-16.

Harff, J., Encyclopedia of Marine Geosciences edited, 2016, 299.

Hudec, Michael R., and Martin PA Jackson. "Terra infirma: Understanding salt tectonics." Earth-Science Reviews 82.1 (2007): 1-28.

Jackson, M. P. A., and Christopher J. Talbot. A glossary of salt tectonics. Bureau of Economic Geology, University of Texas at Austin, 1991.

Janik, T., et al. "Crustal structure across the TESZ along POLONAISE'97 seismic profile P2 in NW Poland." Tectonophysics 360.1 (2002): 129-152.

Kley, J., Franzke, H.J., Jähne, F., Krawczyk, C., Lohr, T., Reicherter, K., Scheck-Wenderoth,M., Sippe, J., Tanner, D., van Gent, H., the SPP Structural Geology Group, 2008. Strain and stress (Chapter 3.3). In: Littke, R., Bayer, U., Gajewski, D., Nelskamp,

S. (Eds.), Dynamics of Complex Intercontinental Basins- the Central European Basin System. Springer- Verlag, Berlin-Heidelberg, pp. 234–245 (ISBN: 978-3-540-85084-7).

Kley, J., Voigt, T., 2008. Late Cretaceous intraplate thrusting in central Europe: effect of Africa- Iberia-Europe convergence, not Alpine collision. Geology 36 (11), 839–842.

Kossow, D., Krawczyk, C., McCann, T., Strecker,M., Negendank, J.F.W., 2000. Style and evolution of salt pillows and related structures in the northern part of the Northeast German Basin. Int. J. Earth Sci. 89, 652–664.

Koyi, Hemin. "The shaping of salt diapirs." Journal of Structural Geology 20.4 (1998): 321-338.

Kraus, Eric B., and Joost A. Businger. Atmosphere-ocean interaction. Vol. 27. Oxford University Press, 1994.

Krauss, M., 1994. The tectonic structure belowthe southern Baltic Sea and its evolution. Z.

Krauss, M., 1994. The tectonic structure belowthe southern Baltic Sea and its evolution. Z. Geol. Wiss. 22, 19–32.

Krauss, M., Mayer, P., 2004. The Vorpommern fault system and its regional structural relationships.

Krawczyk, C. M., et al. "Seismic evidence of Caledonian deformed crust and uppermost mantle structures in the northern part of the Trans-European Suture Zone, SW Baltic Sea." Tectonophysics 360.1 (2002): 215-244.

Krawczyk, C. M., M. Stiller, and DEKORP–BASIN Research Group. "Reflection seismic constraints on Paleozoic crustal structure and Moho beneath the NE German Basin." Tectonophysics 314.1 (1999): 241-253.

Lokhorst, A., Adlam, K., Brugge, J.V.M., David, P., Diapari, L., Fermont, W.J.J., Geluk, M., Gerling, P., Heckers, J., Kockel, F., Kotarba, M., Laier, T., Lott, G.K., Milaczewski, E., Milaczewski, L., Nicholson, R.A., Von Planten, F., Pokorski, J., 1998. NW European Gas Atlas-Composition and Isotope Ratios of Natural Gases. Netherlands Instituutvoor Toegepaste geowetenschappen, Panstwowy Instytut Geologiczny, European Union.

Marek Grad, Timo Tiira & ESC Working Group, University of Helsinki, EUROPEAN PLATE MOHOMAP, Grad, M., Tiira, T. and ESC Working Group (2009), The Moho

depth map of the European Plate. Geophysical Journal International, 176: 279–292. doi:10.1111j.1365-246X.2008.03919.

Maystrenko, Y., Bayer, U., Scheck-Wenderoth, M., 2005a. The Glückstadt Graben, a sedimentary record between the North and Baltic Sea in north Central Europe. Tectonophysics 397 (1–2), 113–126.

Meissner, R., P. Sadowiakl, and S. A. Thomas. "East Avalonia, the third partner in the Caledonian collisions: evidence from deep seismic reflection data." Geologische Rundschau 83.1 (1994): 186-196.

Molinari, I., Morelli, A., 2011. EPcrust: A reference crustal model for the european plate. Geophys. J. Int, 185(1), 352-364, doi: 10.1111/j.1365-246X.2011.04940.x.

NIA-Netherlands Institute of Applied Geoscience TNO, 2000. Northwestern European Gas Atlas, Published on CD-ROM, Utrecht.

Nolet, Guust, and Alet Zielhuis. "Low S velocities under the Tornquist-Teisseyre zone: Evidence for water injection into the transition zone by subduction." Journal of Geophysical Research: Solid Earth 99.B8 (1994): 15813-15820.

Obst, K., Deutschmann, A., 2015. Steps towards a 3D model of the German Baltic Sea area collaboration with academic research in the USO project.

Pharaoh, T. C., et al. "Introduction: geological and geophysical studies in the Trans-European Suture Zone." Geological Magazine 134.5 (1997): 585-590.

Quirk, David G., and Robin S. Pilcher. "Flip-flop salt tectonics." Geological Society, London, Special Publications 363.1 (2012): 245-264.

Reicherter, K., Froitzheim, N., Jarosiski, Badura, J., Franzke, H.-J., Hansen, M.B., Hübscher, C., Müller, R., Poprawa, P., Reinecker, J., Stackebrandt, W., Voigt, H., von Eynatten, H., Zuchiewicz, W., 2008. Alpine tectonics north of the Alps. In: McCann, T. (Ed.), Geology of Central Europe. Special Publication. Geological Society, London.

Reynolds M. Jon, An introduction to applied and environmental Geophysics, 2011 by John Wiey and Sons, Ltd, 19-22.

Schlüter, H.U., Best, G., Jürgens, U., Binot, F., 1997. Interpretation reflexionsseismischer profile zwischen baltischer kontinentalplattes und kaledonisches Becken in der südlichen ostsee-erste Ergebnisse. Z. Dtsch. Geol. Ges. 148 (1), 1–32.

Schlüter, H.U., Jürgens, U., Binot, F., Best, G., 1998. The importance of geological structures

Sea. Z. Dtsch. Geol. Ges. 44 (1).

Thomas, S., Sivhed, U., Erlström, M., Seifert, M., 1993. Seismostratigraphy and structural framework of the SW Baltic Sea. Terra Nova 5, 364–374.

Thybo, Hans. "A seismic model along the EGT profile-from the North German Basin into the Baltic Shield." Proceedings of the 5th Study Centre on the European Geotraverse Project. Esf Strasbourg. 1990. 99-108.

to the Trans-European Fault. Z. Geol. Wiss. 32 (2–4), 227–246.

Vejbæk, O.V., 1997. Dype strukturer I danske sedimentære bassiner. Gelogisk Tidsskrift 4, 1–31.

Vendeville, Bruno C., and Martin PA Jackson. "The rise of diapirs during thin-skinned extension." Marine and Petroleum Geology 9.4 (1992): 331-354.

Weatherall, P., K. M. Marks, M. Jakobsson, T. Schmitt, S. Tani, J. E. Arndt, M. Rovere, D. Chayes, V. Ferrini, and R. Wigley (2015), GEBCO14, A new digital bathymetric model of the world's oceans, Earth and Space Science, 2, 331–345, doi:10.1002/2015EA000107].

Yin, Hongwei, and Richard H. Groshong. "Balancing and restoration of piercement structures: geologic insights from 3D kinematic models." Journal of Structural Geology 28.1 (2006): 99-114.

7. Appendix.

Profile	Coordinates		Anotation	Profile	Coordinates		Anotation
1	54°54‘ ; 13°13‘	55°00‘ ; 13°50‘	W-E	9	54°44‘ ; 12°47‘	54°44‘ ; 14°17‘	W-E
2	54°58‘ ; 13°55‘	54°58‘ ; 13°10‘	W-E	10	54°25‘ ; 13°55‘	54°57‘ ; 13°55‘	N-S
3	54°56‘ ; 13°08‘	54°56‘ ; 14°00‘	W-E	11	55°00‘ ; 13°45‘	54°22‘ ; 13°45‘	N-S
4	54°54‘ ; 14°02‘	54°54‘ ; 13°04‘	W-E	12	54°36‘ ; 13°35‘	55°00‘ ; 13°35‘	N-S
5	54°52‘ ; 13°00‘	54°52‘ ; 14°00‘	W-E	13	55°00‘ ; 13°25‘	55°43‘ ; 13°25‘	N-S
6	54°50‘ ; 14°00‘	54°50‘ ; 12°58‘	W-E	14	54°43‘ ; 13°15‘	54°59‘ ; 13°15‘	N-S
7	54°48‘ ; 12°55‘	54°48‘ ; 14°00‘	W-E	15	55°00‘ ; 13°43‘	54°32‘ ; 12°40‘	NNW-SSE
8	54°46‘; 14°16‘	54°46‘ ; 12°47‘	W-E	16	54°23‘ ; 12°11‘	55°00‘ ; 13°30‘	SSE-NNW
17	54°59 ; 13°50	54°59 ; 13°11	W-E	24	54°45 ; 14°09	54°45 ; 12°50	W-E
18	54°57 ; 13°08	54°57 ; 13°58	W-E	25	54°43 ; 12°46	54°43 ; 14°17	W-E
19	54°55 ; 13°07	54°55 ; 14°00	W-E	26	54°41 ; 14°17	54°41 ; 12°45	W-E
20	54°53 ; 14°09	54°53 ; 13°05	W-E	27	54°57 ; 13°55	54°25 ; 13°55	Profil 10
21	54°51 ; 13°00	54°51 ; 14°00	W-E	28	54°50 ; 13°20	54°50 ; 13°57	OBS-Profil
22	54°49 ; 14°00	54°49 ; 12°56	W-E	29	54°50 ; 13°20	54°50 ; 13°57	OBS (30 s)
23	54°47 ; 12°51	54°47 ; 14°06					

Table 1: List of profiles incl. OBS positions.

```
2016 194 1849 11E 2   555.51 1 0.0019 -0.0001 000000.0 313.30 00.0 T 54 19.787N T010 08.989E 313.30 00.0 0000 0000 0000 0   555.6  -228.7  -228.7
2016 194 1849 12E 2   555.51 1 0.0018 -0.0001 000000.0 098.06 00.0 T 54 19.787N T010 08.989E 098.06 00.0 0000 0000 0000 0   555.6  -228.7  -228.7
2016 194 1849 13E 2   555.52 1 0.0016 -0.0002 000000.0 266.10 00.0 T 54 19.787N T010 08.989E 266.10 00.0 0000 0000 0000 0   555.6  -228.7  -228.7
2016 194 1849 14E 2   555.52 1 0.0015 -0.0002 000000.0 042.12 00.0 T 54 19.787N T010 08.989E 042.12 00.0 0000 0000 0000 0   555.6  -228.7  -228.7
2016 194 1849 15E 2   555.52 1 0.0013 -0.0002 000000.0 211.52 00.1 T 54 19.787N T010 08.989E 211.52 00.1 0000 0000 0000 0   555.6  -228.7  -228.7
2016 194 1849 16E 2   555.52 1 0.0012 -0.0003 000000.0 353.91 00.0 T 54 19.787N T010 08.989E 353.91 00.0 0000 0000 0000 0   555.6  -228.7  -228.7
2016 194 1849 17E 2   555.52 1 0.0010 -0.0003 000000.0 154.62 00.2 T 54 19.787N T010 08.989E 154.62 00.2 0000 0000 0000 0   555.6  -228.7  -228.7
2016 194 1849 19E 2   555.52 1 0.0007 -0.0004 000000.0 102.76 00.1 T 54 19.787N T010 08.989E 102.76 00.1 0000 0000 0000 0   555.6  -228.7  -228.7
2016 194 1849 20E 2   555.52 1 0.0006 -0.0004 000000.0 186.56 00.0 T 54 19.787N T010 08.989E 186.56 00.0 0000 0000 0000 0   555.6  -228.7  -228.7
2016 194 1849 21E 2   555.52 1 0.0005 -0.0005 000000.0 070.13 00.0 T 54 19.787N T010 08.989E 070.13 00.0 0000 0000 0000 0   555.6  -228.7  -228.7
2016 194 1849 22E 2   555.52 1 0.0003 -0.0005 000000.0 156.77 00.1 T 54 19.787N T010 08.989E 156.77 00.1 0000 0000 0000 0   555.6  -228.7  -228.7
2016 194 1849 23E 2   555.52 1 0.0002 -0.0005 000000.0 217.58 00.1 T 54 19.787N T010 08.989E 217.58 00.1 0000 0000 0000 0   555.6  -228.7  -228.7
2016 194 1849 24E 2   555.52 1 0.0000 -0.0006 000000.0 194.22 00.0 T 54 19.787N T010 08.989E 194.22 00.0 0000 0000 0000 0   555.6  -228.7  -228.7
2016 194 1849 25E 2   555.52 1-0.0001 -0.0006 000000.0 021.62 00.1 T 54 19.787N T010 08.989E 021.62 00.1 0000 0000 0000 0   555.6  -228.7  -228.7
2016 194 1849 26E 2   555.52 1-0.0002 -0.0007 000000.0 301.99 00.0 T 54 19.787N T010 08.989E 301.99 00.0 0000 0000 0000 0   555.6  -228.7  -228.7
2016 194 1849 27E 2   555.52 1-0.0003 -0.0007 000000.0 113.20 00.1 T 54 19.787N T010 08.989E 113.20 00.1 0000 0000 0000 0   555.6  -228.7  -228.7
2016 194 1849 29E 2   555.52 1-0.0005 -0.0008 000000.0 181.22 00.0 T 54 19.787N T010 08.989E 181.22 00.0 0000 0000 0000 0   555.6  -228.7  -228.7
2016 194 1849 30E 2   555.52 1-0.0006 -0.0008 000000.0 069.05 00.0 T 54 19.787N T010 08.989E 069.05 00.0 0000 0000 0000 0   555.6  -228.7  -228.7
2016 194 1849 31E 2   555.52 1-0.0007 -0.0009 000000.0 306.67 00.1 T 54 19.787N T010 08.989E 306.67 00.1 0000 0000 0000 0   555.6  -228.7  -228.7
2016 194 1849 32E 2   555.52 1-0.0008 -0.0009 000000.0 041.12 00.0 T 54 19.787N T010 08.989E 041.12 00.0 0000 0000 0000 0   555.6  -228.7  -228.7
2016 194 1849 33E 2   555.52 1-0.0008 -0.0010 000000.0 015.49 00.1 T 54 19.787N T010 08.989E 015.49 00.1 0000 0000 0000 0   555.6  -228.7  -228.7
2016 194 1849 34E 2   555.52 1-0.0009 -0.0010 000000.0 157.25 00.1 T 54 19.787N T010 08.989E 157.25 00.1 0000 0000 0000 0   555.6  -228.7  -228.7
2016 194 1849 35E 2   555.52 1-0.0010 -0.0011 000000.0 078.92 00.0 T 54 19.787N T010 08.989E 078.92 00.0 0000 0000 0000 0   555.6  -228.7  -228.7
2016 194 1849 36E 2   555.52 1-0.0010 -0.0011 000000.0 005.25 00.1 T 54 19.787N T010 08.989E 005.25 00.1 0000 0000 0000 0   555.6  -228.7  -228.7
2016 194 1849 37E 2   555.52 1-0.0010 -0.0011 000000.0 053.76 00.1 T 54 19.787N T010 08.989E 053.76 00.1 0000 0000 0000 0   555.6  -228.7  -228.7
2016 194 1849 38E 2   555.52 1-0.0011 -0.0011 000000.0 147.38 00.2 T 54 19.787N T010 08.989E 147.38 00.2 0000 0000 0000 0   555.6  -228.7  -228.7
2016 194 1849 39E 2   555.52 1-0.0011 -0.0012 000000.0 135.39 00.1 T 54 19.787N T010 08.989E 135.39 00.1 0000 0000 0000 0   555.6  -228.7  -228.7
2016 194 1849 40E 2   555.52 1-0.0011 -0.0012 000000.0 016.54 00.0 T 54 19.787N T010 08.989E 016.54 00.0 0000 0000 0000 0   555.6  -228.7  -228.7
2016 194 1849 41E 2   555.52 1-0.0011 -0.0012 000000.0 283.92 00.0 T 54 19.787N T010 08.989E 283.92 00.0 0000 0000 0000 0   555.6  -228.7  -228.7
2016 194 1849 42E 2   555.52 1-0.0010 -0.0012 000000.0 294.26 00.0 T 54 19.787N T010 08.989E 294.26 00.0 0000 0000 0000 0   555.6  -228.7  -228.7
2016 194 1849 43E 2   555.52 1-0.0010 -0.0012 000000.0 180.24 00.0 T 54 19.787N T010 08.989E 180.24 00.0 0000 0000 0000 0   555.6  -228.7  -228.7
2016 194 1849 44E 2   555.52 1-0.0010 -0.0012 000000.0 161.43 00.0 T 54 19.787N T010 08.989E 161.43 00.0 0000 0000 0000 0   555.6  -228.7  -228.7
2016 194 1849 45E 2   555.52 1-0.0009 -0.0012 000000.0 256.33 00.0 T 54 19.787N T010 08.989E 256.33 00.0 0000 0000 0000 0   555.6  -228.7  -228.7
2016 194 1849 46E 2   555.52 1-0.0009 -0.0012 000000.0 046.44 00.0 T 54 19.787N T010 08.989E 046.44 00.0 0000 0000 0000 0   555.6  -228.7  -228.7
2016 194 1849 47E 2   555.52 1-0.0009 -0.0012 000000.0 088.16 00.0 T 54 19.787N T010 08.989E 088.16 00.0 0000 0000 0000 0   555.5  -228.7  -228.7
2016 194 1849 48E 2   555.52 1-0.0008 -0.0011 000000.0 190.42 00.0 T 54 19.787N T010 08.989E 190.42 00.0 0000 0000 0000 0   555.5  -228.7  -228.7
2016 194 1849 49E 2   555.51 1-0.0008 -0.0011 000000.0 200.68 00.0 T 54 19.787N T010 08.989E 200.68 00.0 0000 0000 0000 0   555.5  -228.7  -228.7
2016 194 1849 50E 2   555.51 1-0.0007 -0.0011 000000.0 078.08 00.0 T 54 19.787N T010 08.989E 078.08 00.0 0000 0000 0000 0   555.5  -228.7  -228.7
2016 194 1849 51E 2   555.51 1-0.0007 -0.0011 000000.0 260.54 00.0 T 54 19.787N T010 08.989E 260.54 00.0 0000 0000 0000 0   555.5  -228.7  -228.7
2016 194 1849 53E 2   555.51 1-0.0005 -0.0011 000000.0 004.47 00.1 T 54 19.787N T010 08.989E 004.47 00.1 0000 0000 0000 0   555.5  -228.7  -228.7
2016 194 1849 54E 2   555.50 1-0.0005 -0.0011 000000.0 122.90 00.0 T 54 19.787N T010 08.989E 122.90 00.0 0000 0000 0000 0   555.5  -228.7  -228.7
2016 194 1849 55E 2   555.50 1-0.0004 -0.0011 000000.0 079.23 00.2 T 54 19.787N T010 08.989E 079.23 00.2 0000 0000 0000 0   555.5  -228.7  -228.7
2016 194 1849 56E 2   555.50 1-0.0004 -0.0010 000000.0 163.90 00.0 T 54 19.787N T010 08.989E 163.90 00.0 0000 0000 0000 0   555.5  -228.7  -228.7
2016 194 1849 57E 2   555.50 1-0.0003 -0.0010 000000.0 194.54 00.1 T 54 19.787N T010 08.989E 194.54 00.1 0000 0000 0000 0   555.5  -228.7  -228.7
```

Table 2: The gravimetric data without processing.

2016/07/13	05:00:00	010	08.99	E	54	19.79	N	7.6	15.0	0.0 DGPS1	0.0000
2016/07/13	05:00:01	010	08.99	E	54	19.79	N	7.6	14.0	0.0 DGPS1	0.0000
2016/07/13	05:00:02	010	08.99	E	54	19.79	N	7.6	15.0	0.0 DGPS1	0.0000
2016/07/13	05:00:03	010	08.99	E	54	19.79	N	7.6	16.0	0.0 DGPS1	0.0000
2016/07/13	05:00:04	010	08.99	E	54	19.79	N	7.6	16.0	0.0 DGPS1	0.0000
2016/07/13	05:00:05	010	08.99	E	54	19.79	N	7.6	18.0	0.0 DGPS1	0.0000
2016/07/13	05:00:06	010	08.99	E	54	19.79	N	7.6	18.0	0.0 DGPS1	0.0000
2016/07/13	05:00:07	010	08.99	E	54	19.79	N	7.6	20.0	0.0 DGPS1	0.0000
2016/07/13	05:00:08	010	08.99	E	54	19.79	N	7.6	19.0	0.0 DGPS1	0.0000
2016/07/13	05:00:09	010	08.99	E	54	19.79	N	7.6	17.0	0.0 DGPS1	0.0000
2016/07/13	05:00:10	010	08.99	E	54	19.79	N	7.6	12.0	0.0 DGPS1	0.0000
2016/07/13	05:00:11	010	08.99	E	54	19.79	N	7.6	6.0	0.0 DGPS1	0.0000
2016/07/13	05:00:12	010	08.99	E	54	19.79	N	7.6	5.0	0.0 DGPS1	0.0000
2016/07/13	05:00:13	010	08.99	E	54	19.79	N	7.6	5.0	0.0 DGPS1	0.0000
2016/07/13	05:00:14	010	08.99	E	54	19.79	N	7.6	5.0	0.0 DGPS1	0.0000
2016/07/13	05:00:15	010	08.99	E	54	19.79	N	7.3	5.0	0.0 DGPS1	0.0000
2016/07/13	05:00:16	010	08.99	E	54	19.79	N	7.6	6.0	0.0 DGPS1	0.0000
2016/07/13	05:00:17	010	08.99	E	54	19.79	N	7.6	6.0	0.0 DGPS1	0.0000
2016/07/13	05:00:18	010	08.99	E	54	19.79	N	7.6	3.0	0.0 DGPS1	0.0000
2016/07/13	05:00:19	010	08.99	E	54	19.79	N	7.6	7.0	0.0 DGPS1	0.0000
2016/07/13	05:00:20	010	08.99	E	54	19.79	N	7.6	10.0	0.0 DGPS1	0.0000
2016/07/13	05:00:21	010	08.99	E	54	19.79	N	7.6	11.0	0.0 DGPS1	0.0000
2016/07/13	05:00:22	010	08.99	E	54	19.79	N	7.6	14.0	0.0 DGPS1	0.0000
2016/07/13	05:00:23	010	08.99	E	54	19.79	N	7.4	15.0	0.0 DGPS1	0.0000
2016/07/13	05:00:24	010	08.99	E	54	19.79	N	7.6	10.0	0.0 DGPS1	0.0000
2016/07/13	05:00:25	010	08.99	E	54	19.79	N	7.6	10.0	0.0 DGPS1	0.0000
2016/07/13	05:00:26	010	08.99	E	54	19.79	N	7.6	13.0	0.0 DGPS1	0.0000
2016/07/13	05:00:27	010	08.99	E	54	19.79	N	7.6	13.0	0.0 DGPS1	0.0000
2016/07/13	05:00:28	010	08.99	E	54	19.79	N	7.6	14.0	0.0 DGPS1	0.0000
2016/07/13	05:00:29	010	08.99	E	54	19.79	N	7.6	14.0	0.0 DGPS1	0.0000
2016/07/13	05:00:30	010	08.99	E	54	19.79	N	7.6	14.0	0.0 DGPS1	0.0000
2016/07/13	05:00:31	010	08.99	E	54	19.79	N	7.6	12.0	0.0 DGPS1	0.0000
2016/07/13	05:00:32	010	08.99	E	54	19.79	N	7.6	12.0	0.0 DGPS1	0.0000
2016/07/13	05:00:33	010	08.99	E	54	19.79	N	7.6	13.0	0.0 DGPS1	0.0000
2016/07/13	05:00:34	010	08.99	E	54	19.79	N	7.6	14.0	0.0 DGPS1	0.0000
2016/07/13	05:00:35	010	08.99	E	54	19.79	N	7.6	14.0	0.0 DGPS1	0.0000
2016/07/13	05:00:36	010	08.99	E	54	19.79	N	7.6	15.0	0.0 DGPS1	0.0000
2016/07/13	05:00:37	010	08.99	E	54	19.79	N	7.6	16.0	0.0 DGPS1	0.0000
2016/07/13	05:00:38	010	08.99	E	54	19.79	N	7.6	16.0	0.0 DGPS1	0.0000
2016/07/13	05:00:39	010	08.99	E	54	19.79	N	7.6	16.0	0.0 DGPS1	0.0000
2016/07/13	05:00:40	010	08.99	E	54	19.79	N	7.6	15.0	0.0 DGPS1	0.0000
2016/07/13	05:00:41	010	08.99	E	54	19.79	N	7.6	15.0	0.0 DGPS1	0.0000
2016/07/13	05:00:42	010	08.99	E	54	19.79	N	7.3	15.0	0.0 DGPS1	0.0000
2016/07/13	05:00:43	010	08.99	E	54	19.79	N	7.6	16.0	0.0 DGPS1	0.0000

Table 3: The bathymetric and navigational data.

Year	n/d	time	grav	longitude	latitude	course	speed	depth
2016	195	4 59 59	553.40	54.32983	10.14983	15.00	.00	7.6
2016	195	5 0 0	553.40	54.32983	10.14983	14.00	.00	7.6
2016	195	5 0 2	553.40	54.32983	10.14983	15.00	.00	7.6
2016	195	5 0 3	553.40	54.32983	10.14983	16.00	.00	7.6
2016	195	5 0 4	553.40	54.32983	10.14983	16.00	.00	7.6
2016	195	5 0 5	553.40	54.32983	10.14983	18.00	.00	7.6
2016	195	5 0 6	553.40	54.32983	10.14983	18.00	.00	7.6
2016	195	5 0 7	553.40	54.32983	10.14983	20.00	.00	7.6
2016	195	5 0 8	553.30	54.32983	10.14983	19.00	.00	7.6
2016	195	5 0 9	553.30	54.32983	10.14983	17.00	.00	7.6
2016	195	5 0 10	553.30	54.32983	10.14983	12.00	.00	7.6
2016	195	5 0 12	553.30	54.32983	10.14983	6.00	.00	7.6
2016	195	5 0 13	553.30	54.32983	10.14983	5.00	.00	7.6
2016	195	5 0 14	553.30	54.32983	10.14983	5.00	.00	7.6
2016	195	5 0 15	553.30	54.32983	10.14983	5.00	.00	7.3
2016	195	5 0 16	553.30	54.32983	10.14983	6.00	.00	7.6
2016	195	5 0 17	553.30	54.32983	10.14983	6.00	.00	7.6
2016	195	5 0 18	553.30	54.32983	10.14983	3.00	.00	7.6
2016	195	5 0 19	553.30	54.32983	10.14983	7.00	.00	7.6
2016	195	5 0 20	553.30	54.32983	10.14983	10.00	.00	7.6
2016	195	5 0 22	553.30	54.32983	10.14983	14.00	.00	7.6
2016	195	5 0 23	553.30	54.32983	10.14983	15.00	.00	7.4
2016	195	5 0 24	553.30	54.32983	10.14983	10.00	.00	7.6
2016	195	5 0 25	553.30	54.32983	10.14983	10.00	.00	7.6
2016	195	5 0 26	553.30	54.32983	10.14983	13.00	.00	7.6
2016	195	5 0 27	553.30	54.32983	10.14983	13.00	.00	7.6
2016	195	5 0 28	553.30	54.32983	10.14983	14.00	.00	7.6
2016	195	5 0 29	553.20	54.32983	10.14983	14.00	.00	7.6
2016	195	5 0 30	553.20	54.32983	10.14983	14.00	.00	7.6
2016	195	5 0 31	553.10	54.32983	10.14983	12.00	.00	7.6
2016	195	5 0 32	553.10	54.32983	10.14983	12.00	.00	7.6
2016	195	5 0 32	553.20	54.32983	10.14983	13.00	.00	7.6
2016	195	5 0 34	553.20	54.32983	10.14983	14.00	.00	7.6
2016	195	5 0 35	553.20	54.32983	10.14983	14.00	.00	7.6
2016	195	5 0 36	553.20	54.32983	10.14983	15.00	.00	7.6
2016	195	5 0 37	553.20	54.32983	10.14983	16.00	.00	7.6
2016	195	5 0 38	553.20	54.32983	10.14983	16.00	.00	7.6
2016	195	5 0 39	553.20	54.32983	10.14983	16.00	.00	7.6
2016	195	5 0 40	553.20	54.32983	10.14983	15.00	.00	7.6
2016	195	5 0 41	553.20	54.32983	10.14983	15.00	.00	7.6
2016	195	5 0 42	553.20	54.32983	10.14983	15.00	.00	7.3
2016	195	5 0 43	553.20	54.32983	10.14983	16.00	.00	7.6
2016	195	5 0 44	553.20	54.32983	10.14983	19.00	.00	7.6
2016	195	5 0 45	553.20	54.32983	10.14983	18.00	.00	7.6

Table 4: combined the gravity data with the bathymetric data, the file “gn481”.

Year	n/d	time	longitude	latitude	course	speed	depth	Free-air	Bouguer
2016	195	13 56 14	12.62117	54.64900	59.0	12.6	18.0	2.40	3.66
2016	195	13 56 15	12.62133	54.64900	59.0	12.6	18.0	2.40	3.66
2016	195	13 56 17	12.62133	54.64900	59.0	12.6	18.0	2.40	3.66
2016	195	13 56 17	12.62150	54.64900	59.0	12.6	18.0	2.40	3.66
2016	195	13 56 18	12.62150	54.64917	59.0	12.6	18.0	2.39	3.65
2016	195	13 56 19	12.62167	54.64917	59.0	12.6	18.0	2.39	3.65
2016	195	13 56 20	12.62167	54.64917	59.0	12.6	18.0	2.39	3.65
2016	195	13 56 21	12.62183	54.64917	59.0	12.6	18.0	2.29	3.55
2016	195	13 56 22	12.62183	54.64917	59.0	12.6	18.0	2.29	3.55
2016	195	13 56 23	12.62217	54.64933	59.0	12.6	18.0	2.27	3.53
2016	195	13 56 26	12.62217	54.64933	59.0	12.6	18.0	2.17	3.43
2016	195	13 56 27	12.62233	54.64933	58.0	12.6	18.0	1.67	2.93
2016	195	13 56 28	12.62233	54.64933	58.0	12.6	18.0	1.67	2.93
2016	195	13 56 29	12.62250	54.64950	58.0	12.6	18.0	1.56	2.82
2016	195	13 56 30	12.62250	54.64950	58.0	12.6	18.1	1.56	2.83
2016	195	13 56 31	12.62283	54.64950	58.0	12.6	18.0	1.56	2.82
2016	195	13 56 34	12.62283	54.64950	58.0	12.6	18.1	1.46	2.73
2016	195	13 56 35	12.62317	54.64967	58.0	12.6	18.0	1.44	2.70
2016	195	13 56 38	12.62317	54.64967	58.0	12.6	18.0	1.44	2.70
2016	195	13 56 39	12.62333	54.64967	58.0	12.6	18.0	1.44	2.70
2016	195	13 56 40	12.62333	54.64983	58.0	12.6	18.0	1.43	2.69
2016	195	13 56 43	12.62367	54.64983	59.0	12.6	18.0	1.93	3.19
2016	195	13 56 44	12.62367	54.64983	59.0	12.6	18.0	1.93	3.19
2016	195	13 56 47	12.62400	54.65000	59.0	12.6	18.1	1.92	3.18
2016	195	13 56 48	12.62417	54.65000	59.0	12.6	18.1	1.92	3.18
2016	195	13 56 51	12.62433	54.65017	59.0	12.6	18.1	1.90	3.17
2016	195	13 56 52	12.62450	54.65017	59.0	12.6	18.1	1.90	3.17
2016	195	13 56 53	12.62450	54.65017	59.0	12.6	18.1	1.90	3.17
2016	195	13 56 54	12.62467	54.65017	59.0	12.6	18.1	1.90	3.17
2016	195	13 56 55	12.62467	54.65017	59.0	12.6	18.1	1.90	3.17
2016	195	13 56 56	12.62483	54.65017	59.0	12.6	18.1	1.90	3.17
2016	195	13 56 57	12.62483	54.65033	59.0	12.6	18.1	1.89	3.15
2016	195	13 56 59	12.62500	54.65033	59.0	12.6	18.1	1.89	3.15
2016	195	13 56 59	12.62517	54.65033	59.0	12.6	18.1	1.89	3.15
2016	195	13 57 0	12.62517	54.65033	59.0	12.6	18.1	1.89	3.15
2016	195	13 57 2	12.62533	54.65050	59.0	12.6	18.1	1.87	3.14
2016	195	13 57 3	12.62533	54.65050	59.0	12.6	18.1	1.87	3.14
2016	195	13 57 4	12.62550	54.65050	59.0	12.6	18.1	1.87	3.14
2016	195	13 57 5	12.62550	54.65050	58.0	12.6	18.1	1.37	2.64
2016	195	13 57 7	12.62567	54.65050	58.0	12.6	18.1	1.27	2.54
2016	195	13 57 8	12.62583	54.65067	58.0	12.6	18.1	1.26	2.52
2016	195	13 57 11	12.62600	54.65067	58.0	12.6	18.0	1.26	2.52
2016	195	13 57 12	12.62617	54.65067	58.0	12.6	18.1	1.26	2.52
2016	195	13 57 13	12.62617	54.65083	58.0	12.6	18.1	1.24	2.51
2016	195	13 57 14	12.62633	54.65083	58.0	12.6	18.1	1.24	2.51

Table 5: The file **"fb481"** with the counted the "Free-air" and "Bouguer" anomalies data.

Statement on the thesis' originality.

Herewith I, Mikhail Vladimirov, declare that I wrote the thesis independently and did not use any other resources than those named in the bibliography, and, in particular, did not use any internet resources except for those named in the bibliography. The master thesis has not been used previously as part of an examination. The master thesis has not been previously published.